



MONASH University

Dual-Function Smart Electrolytes for Novel Design of Dye-Sensitized Solar Cells

Rishabh Bhargava
Integrated M. Tech Nanotechnology

A thesis submitted for the degree of *Masters by Research* at
Monash University in *2016*
Materials Engineering

Copyright Notice

© The author, Rishabh Bhargava (2016). Except as provided in the Copyright Act 1968, this thesis may not be reproduced in any form without the written permission of the author.

Abstract

Dual-Function Smart Electrolyte for Dye-Sensitized Solar Cells: 5-Mercaptotetrazoles as Redox Mediator and Corrosion Inhibitor

Investigated derivatives of 5-mercaptotetrazoles as redox mediator in DSCs and corrosion inhibitors for metal charge collectors employed in large scale DSCs and observed that structural modifications in the 5-mercaptotetrazoles lead to differences in corrosion inhibition properties. Four wire sense measurement and cyclic voltammetry were utilized as characterization tools for characterizing the corrosion inhibition and suppression of recombination by 5-mercaptotetrazoles at the silver metal - electrolyte interface. The results were compared with standard iodine and cobalt based electrolytes. Rate of corrosion was two orders of magnitude lesser for the phenyl based 5-mercaptotetrazole derivative electrolyte compared to standard iodine and cobalt based electrolytes (0.2 nm/hr vs >3600 $\mu\text{m/hr}$ respectively). STM measurements were carried out to characterize^[1] the coverage of the silver metal surface by the derivatives of 5-mercaptotetrazoles. Depending on the structure a dense monolayer could be achieved. Small and large area solar cells were fabricated utilizing the 5-mercaptotetrazoles as redox mediator and a proof of principle device achieved reasonable efficiency.

Application of thiolate based electrolyte in development of ptype DSC and pn-DSC

In addition, 5-methyl mercaptotetrazoles based electrolyte(T_{ph}) was also investigated in p-type and pn-DSCs. We observed that applying these thiolate based electrolytes resulted in an improvement in VOC in p-DSCs compared to the devices based on iodide electrolytes, while maintaining similar JSC (5.3 mA/cm²) values. We also employed the T_{ph} electrolyte in tandem DSCs with film thicknesses optimized for both the T_{ph} and Iodine based electrolytes, we observed that the tandem cells based on the non-corrosive thiolate electrolyte exhibited similar conversion efficiencies (1.33 %) to those based on iodide electrolytes (1.28 %). Our results reveal the great promise which the thiolate based electrolytes holds for future applications in p-DSCs and pn-DSCs.

Declaration

This thesis contains no material which has been accepted for the award of any other degree or diploma at any university or equivalent institution and that, to the best of my knowledge and belief, this thesis contains no material previously published or written by another person, except where due reference is made in the text of the thesis.

Publications during enrolment

1. Dual-Function Smart Electrolyte for Dye-Sensitized Solar Cells: 5-Mercaptotetrazoles as Redox Mediator and Corrosion Repressor
2. Thiolate/Disulfide Based Electrolytes for p-type and Tandem Dye-Sensitized Solar Cells

Thesis including published works General Declaration

I hereby declare that this thesis contains no material which has been accepted for the award of any other degree or diploma at any university or equivalent institution and that, to the best of my knowledge and belief, this thesis contains no material previously published or written by another person, except where due reference is made in the text of the thesis.

This thesis includes 2 original papers published in peer reviewed journals. The core theme of the thesis is Dual Function Smart Electrolyte for application in Dye Sensitised Solar Cells. The ideas, development and writing up of all the papers in the thesis were the principal responsibility of myself, the candidate, working within the *Materials Engineering* under the supervision of Udo Bach

The inclusion of co-authors reflects the fact that the work came from active collaboration between researchers and acknowledges input into team-based research.

In the case of *appendix chapter*, my contribution to the work involved the following:

Developing thiolate based electrolyte for experimentation purposes.

Thesis chapter	Publication title	Publication status*	Nature and extent (%) of students contribution
Chapter 3	Dual-Function Smart Electrolyte for Dye-Sensitized Solar Cells: 5-Mercaptotetrazoles as Redox Mediator and Corrosion Repressor	Published	60
Appendix	Thiolate/Disulfide Based Electrolytes for p-type and Tandem Dye-Sensitized Solar Cells	Published	10

I have not renumbered sections of published papers in order to generate a consistent presentation within the thesis.

Student signature:



Date: 14.12.15

The undersigned hereby certify that the above declaration correctly reflects the nature and extent of the student and co-authors' contributions to this work.

Main Supervisor signature:



Date: 13.01.16

Acknowledgements

Numerous people and events that happened during the period in which I did my research made this thesis possible. Firstly I would like to thank my main supervisor Professor Udo Bach, who was a constant source of guidance and support. I remember coming to Monash for the first time in 2010 for an interview while I was doing my master thesis at Deakin University Geelong. I was quite nervous, but he had put me at ease right from the beginning and I knew, I would gain and learn a lot from him, which I did. In spite of not getting selected in 2010 for the PhD during the Graduate Research application rounds, he still supported my application and he took me on as a PhD student for the VICOSC project in 2011. I have learnt a lot from him. Right from the basic tools of research to doing physical chemistry experiments to understanding how dye sensitized solar cells work. It was always mentally stimulating when he would explain scientific concepts. I have told him quite often that the amount I have learnt from you, I never did in five years of my integrated masters degree in India and I still stand by it.

Udo not just supported me academically but was very supportive during my battle with cancer. He backed me to the hilt and helped me in completing my first year confirmation, my very first research paper, getting all the documentation work needed to apply for leave or getting my PhD converted to Masters by Research degree while I fought with the disease.

I also want to thank Professor Yi Bing and Professor Leone Spiccia who were always there to provide their valuable guidance and support whether conceptually or some experiments needed to be arranged in other departments. They have been very supportive with their inputs during my research and which is what has helped in formulating the theories and the corroborating experiments that I did in laboratory.

Furthermore, I would like to thank Dr Torben Daeneke, without whom, this thesis would have never been completed. He was my man Friday or go to man whenever I had any doubts either conceptually or experimentally. He was like a pseudo guide for

me. He is one patient man who would hear me out and try and resolve my issues. Besides the professional expertise, he is also a very close friend with whom I would go around Monash during breaks having discussions about life and everything in it. I thank him from the bottom of my heart for being there for me through thick and thin.

I would also like to thank Dr Simon Thompson. The fun human being who like Torben is also a very close friend and who has helped me a lot professionally on how to do experiments properly and taught me a lot of conceptual things which have helped me and saved me a lot of time when I did experiments. His famous words being, “you have to learn on how to do things smartly so that you always have time to go and have lunch!” he was my hangout buddy with whom I would go for movies, learn surfing or rather trying to, go and eat and top it off with ice cream.

I also want to thank my two dear colleagues, Dr Satvasheel Powar and Ishanie Illeperuma, with whom I have a wonderful personal and professional equation. Satvasheel was and still is a happy go lucky person and his enthusiasm and laughter would lighten up not just the lab atmosphere but even social gatherings. He is somebody who would just help you enjoy your work. Ishanie is a wonderful and a kind human being with whom I shared a very warm rapport, who would be there to help not just professionally but also personally. I have always admired her professional conduct and how very well organized she is while doing her research. Observing her made me also consciously make an effort to be more organized in my research.

I also want to thank my fellow colleagues, Dr Wanchun Xiang, Dr Dongchuan Fu, Dr Bofei Xu, Dr Jiangjing He, Dr Yu Ha and Dr Fuzhi Huang who supported me and helped me in doing my lab experiments but were also my fellow badminton colleagues and champions in their own right.

I also want to thank my other colleagues, Dr Kalim Kashif, Rebecca Milhuesen, Isabela Castro, Dr Philip Reineck, Alex Pascoe, Yasmina Dkhissi, Dr George Lee, Anuradha Sepalge, Dr Monika Fekete, Kedar Deshmukh, Nahid and also Dr Chris McNeill for their help and discussions during the course of my research.

I want to thank my parents, who were supportive of sending me abroad and encouraging me to do my higher studies. They have been a constant support throughout my life and are my backbone and will continue to remain so.

I want to thank my housemates Deepak and Sonia Khatter for their wonderful support and home, which I made my home as well for 3 years since I came to Australia. I also want to thank my batchmates from Amity University who came to Australia like me to do PhD, Hitesh Pingle, Akash Bachhuka, Karan Gulati and Tushar Kumeria for their support.

I would also like to thank Dr David Speakman and his wonderful colleagues, who treated me at Peter Mac Cancer Hospital for their immense support care and confidence in me of fighting this disease and beating it.

Last but not the least, the most important person in my life and still is, Dr Rakshita Khanijou, without whom I would have lost my sanity either while doing my research or my battle with cancer. She has been a pillar of strength for me from 10000 km away during my trying times in Australia. If I stand today as a stronger and a braver person, it is due to her faith in me and her prayer and love for me. I couldn't have done it without you.

TABLE OF CONTENTS

COPYRIGHT NOTICE.....	I
ABSTRACT.....	II
DECLARATION	III
Acknowledgements	vi
CHAPTER 1.....	1
LITERATURE REVIEW PART 1: INTRODUCTION	
CHAPTER 2.....	6
Literature Review Part 2 : Redox Electrolytes, Corrosion Inhibitor, Counter Electrodes, DSC Module Designs and Scope Of This Thesis	
CHAPTER 3	20
Dual Function Smart Electrolytes For Novel Design of Dye Sensitized Solar Cells: 5-Mercaptotetrazoles as Redox Mediator and Corrosion Repressor	
CHAPTER 4.....	41
Future Work And Conclusion	
CHAPTER 5:	48
Thiolate/Disulfide Based Electrolytes for p-type and Tandem Dye-Sensitized Solar Cells	

CHAPTER 1

Literature Review Part 1: Introduction

Literature Review: Introduction

World energy demands are increasing with our ever expanding population and rapidly growing global industrialization thus putting a high demand on our natural resources which is expected to double in the next few years^[3]. Fossil fuels cover ~ 85% of energy production worldwide, but the resources are limited. The reserves of fossil fuels throughout the whole world in 2002 were projected to last 40 years for oil, 60 years for natural gas and 200 years for coal.^[3] Thus alternate renewable energy sources such as solar energy production are fast becoming a vital cog for an alternative and sustainable source of energy to replace traditional fossil fuel-based power sources. The most efficient solar cells today are based on crystalline silicon wafers having practical energy-conversion efficiencies of 25 %.^[4] However, they are thick and brittle, expensive, and require significant energy in their manufacture (1 kW of electricity to make a 1W solar cell).^[5] In the past, the development of alternative next-generation solar cells have been tried, including thin film solar cells, amorphous silicon solar cells, dye-sensitized solar cells (DSCs) and organic polymer solar cells. Of these, DSCs have attained reasonable efficiency (12% in laboratory), the lowest material costs and simplest manufacturing process.^[6]

DSCs are made of (i) interconnected semiconductor nanoparticles coated with organic dyes and (ii) a liquid electrolyte that immerses the semiconductor nanostructure (Fig. 1). In their operation, *sunlight is converted to electrons and holes by dye molecules*. The interconnected semiconductor nanoparticles form a *nanoporous structure* that offers a high surface area to help capture much of the sunlight, contributing to the high energy-conversion efficiency. The photo-generated electrons are injected into the interconnected semiconductor nanoparticles (that acts as a “working electrode”) and transferred to the anode. TiO_2 nanoparticles are commonly used as a working electrode, due to a high surface area and a suitable band gap energy level. The photo-generated holes are transferred to the

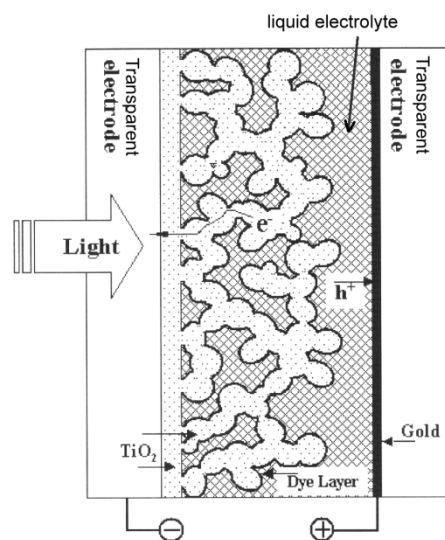


Fig. 1. Typical structure of dye sensitized solar cells

liquid electrolyte and ultimately to the cathode. With the progress and breakthroughs achieved in the field of nanotechnology, it has opened up new avenues for these type of systems.^[7]

Much research on DSCs is dedicated to the improvement of their efficiency. However, critical issues for the commercialization of DSCs, regardless of the efficiency of the cells, are mainly caused by the liquid electrolyte.^[8] Iodine-based liquid electrolytes, that are essential to the current design of DSCs, are volatile, highly corrosive and absorb in the visible region of light.^[9] *“Also when we scale up the DSCs into making large modules, if the liquid electrolytes come into contact with current collectors of silver (Ag) collection fingers in parallel-connected modules, it can give rise to oxidation of Ag and thereby to an increase in series resistance and even worse, to the eventual complete depletion of I_3^- and thus performance. For instance, 100 mM of I_3^- in a 40-micron thick electrolyte layer would be entirely consumed by a corrosion current of 2.5 nA/cm^2 over a year. Thus for a product life of 20 years, average corrosion currents should not be much larger than 0.1 nA/cm^2 , a level that has been shown to be achievable with common insulating films”.*^[9]

All the different module designs have one commonality i.e. employing sealants to protect the silver grids. So far, 4 main types of sealants have been investigated for both cells and modules, which are:

- Elastomeric polymers
- Thermoplastic polymers
- Glass frits
- Adhesives (epoxy etc.)

Arakawa et al. reported successful protection of silver grids in a 10 cm x 10 cm p-design module by employing combination of glass frits and polymer over layers^[10]. Glass frits have also been employed successfully by Dyesol in 1995 to protect the silver grids but it required multiple applications, as the frits couldn't be used with rough high conductivity TCOs due to leakage of electrolyte under the glass-TCO seal.^[9]

Therefore we see a need to address and solve the problem of adequately protecting the silver grids from the corrosive nature of iodide triiodide electrolytes and this study investigates looking into alternative electrolytes that would be able to give reasonable efficiency and mainly solve the problem of protecting the silver grids without the use of a sealant and thus reduce one step in manufacturing and reducing cost of modules. Much research on DSCs is dedicated to the improvement of their efficiency. However, critical issues for the commercialization of DSCs, regardless of the efficiency of the cells, are mainly caused by the liquid electrolyte^[11]. Iodine-based and cobalt based liquid electrolytes, that are essential to the current design of DSCs, are volatile, highly corrosive and absorb in visible region of light^[11].

Their corrosiveness to metal charge collectors gives a major incentive for researching alternative redox mediators. Their corrosiveness complicates the design of large area DSC modules, since an additional step of protecting the metal charge collection electrodes (typically silver) by employing protective sealants, such as epoxy, polymer sealants, glass frits etc. is needed^[11]. These sealants are necessary since direct contact between the I^-/I_3^- and silver will lead to the depletion of triiodide as well as the rapid corrosion of the metal, increasing the series resistance of the device^[12]. A second impediment for the application of metallic charge collectors in photoelectrochemical solar cells is the low over potential exhibited by most redox mediators on these metals as direct contact of the electrolyte with metallic charge collectors located on the photoanode would result in significant recombination losses across the metal-electrolyte interface.

In 2010, Wang et al. introduced an electrolyte based on 5-mercapto-1-methyltetrazole and di-5- (1-methyltetrazole) disulfide^[13]. Following this landmark paper, a number of other thiolate-based electrolytes were studied^[1]. These alternative electrolytes have been promising in terms of overall DSC performance, but the inhibition of corrosive processes in DSCs has not been studied in detail^[14]. Thiolates are, however, well known corrosion inhibitors due to their ability to form strong metal – thiolate bonds^[15].

By applying a suitable thiolate / disulfide redox couple in DSCs, we can take advantage of the strong metal-thiolate interaction, designing a smart electrolyte that passivates metal surfaces within the solar cell while also mediating the charge transport and dye regeneration processes, and potentially eliminating complicated and error prone silver protection steps.

Ultimately the aim is to find a suitable metal that should be corrosion resistant in contact with a suitable thiolate based electrolyte, cheaper than silver while offering similar conductivity and robustness. This would allow reducing the costs of manufacturing DSCs on large scale^[1]. Another impediment of the current DSC design is the use of TCO substrates (transparent conducting oxide), which is the main cost contributor for the manufacture of DSCs^[1]. TCO free substrates for DSCs have been developed but have employed vacuum processes and etching methods, which are not feasible for large scale printing of DSCs^[1]. Also, the current high efficiencies of DSCs have been achieved on TCO based substrates. One ultimate aim of this work is a fully printed TCO free DSC module, which would make manufacturing cheaper and more feasible.

CHAPTER 2

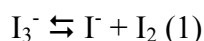
Literature Review Part 2: Redox Electrolytes, Corrosion Inhibitors, Counter Electrodes and DSC Module Designs

Literature Review:

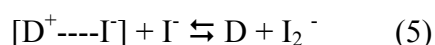
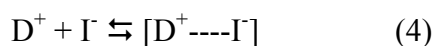
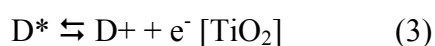
2.1 Redox Electrolytes

2.1.1 Iodide – triiodide

The standard redox couple is iodide- triiodide. Efficiencies as high as 11.4% and 9.9 % have been reported using this redox mediator in lab-based devices and in larger modules respectively.^[4, 16] It is a two electron redox couple. The electrolyte is prepared by mixing iodine with an iodide salt typically in an organic solvent. The triiodide ion is formed as per the following reaction:



In a conventional DSC, the charge separation and dye regeneration occur as per the following equations:



The photoexcited dye (equation 2) releases an electron into the conduction band of TiO_2 (equation 3). The dye is then reduced under the formation of an adduct of dye-iodide (equation 4). The adduct then has to further react with another iodide ion to be able to regenerate the dye back to its ground state and form a I_2^- radical (equation 5). Two I_2^- then form I_3^- and I^- ions.^[17] This electrolyte system was first introduced in 1991 by Grätzel and co workers.^[6a] and since then many electrolyte systems have been introduced but with comparable or lesser efficiencies and the research on alternate electrolytes is still ongoing.^[2, 18]

The reason for looking at alternate electrolytes is due to certain disadvantages of the iodide-triiodide redox couple. One of them is that I_2 is volatile and may escape if the solar cell seal is damaged. Further the complex regeneration mechanism as highlighted in equation 2 through to equation 6 is a limiting factor of the iodide-triiodide redox couple.

The present study is more focused on the other drawbacks of the iodide-triiodide redox couple that are firstly, it absorbs strongly in visible spectrum of light. The I_3^- absorbs below 500 nm competing with the dye for photons. The other drawback being that this redox couple is highly corrosive in nature. To fabricate large DSC modules we require metal charge collection grids on conductive glass substrates that reduce the series resistance losses. One of the main metals used for such grids is silver. The I_3^- ion when it comes in contact with silver would completely oxidize the metal and also deplete the I_3^- concentration and thus increase series resistance and worsen the performance of modules. This leads to complications in designing large-scale modules.

2.1.2 Thiolate/ Disulfide

As concluded in the previous paragraph, that the iodide- triiodide redox couple corrodes the silver metal and absorbs in visible spectrum of light, therefore it is of paramount importance to look into alternative electrolytes, which can inhibit corrosion of silver metal.

The thiolate/disulfide is a new class of two electron redox couples which have been receiving an increased attention since they were first reported in 2010.^[19] Wang et al. showed that the tetramethylammonium salt of 5-mercaptopotrazole (T^-) and 5,5' – dithiobis (1-methyl-1H-tetrazole) (T_2) can be used as a redox mediator in a DSC electrolyte to achieve a 6.4% efficiency. This value got further enhanced to 7.9% when an alternate counter electrode material PEDOT was utilized^[20]. The redox potential of thiolate/ disulfide is similar to that of iodide-triiodide redox couple. Although it is also a two electron redox couple but the electron loss reaction through recombination between the oxidized species and injected electrons is slower.^[13] There have been several analogs reported which have shown high efficiencies, including the

amino acid L-cysteine achieving 7.7%. Also one very recent paper has employed the same class of thiolate/ disulfide based redox electrolyte used in this study and achieved 6% efficiency and utilized for making a bifacial solar cell^[1a, 1c, 14, 21]. The reaction mechanism scheme (figure 2) has also been discussed and compared our class of electrolyte with the one published by Wang et al in 2010.

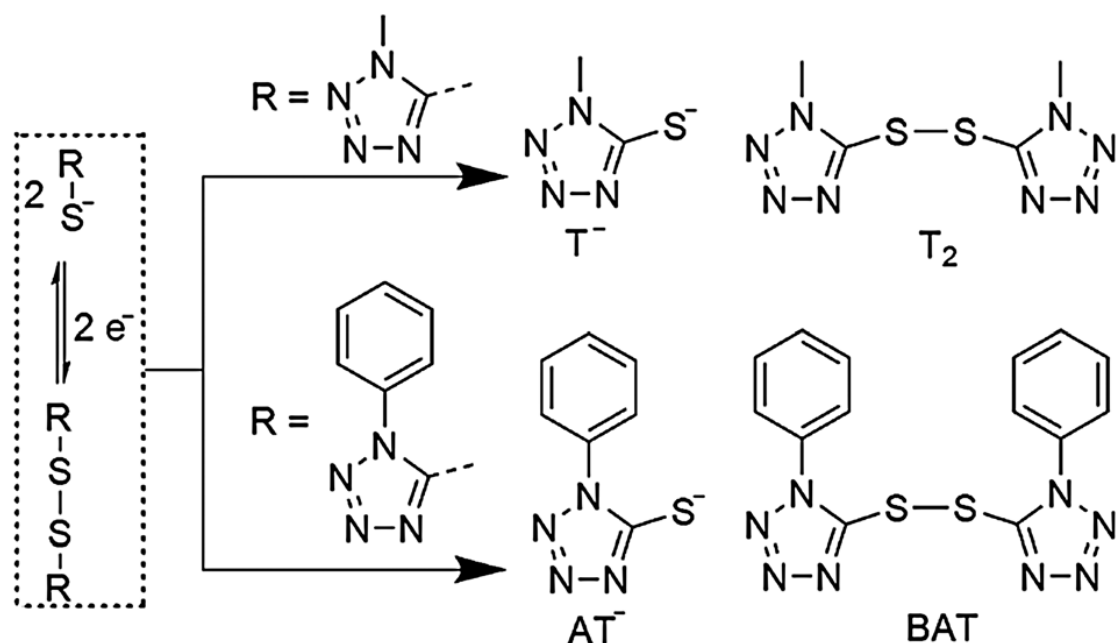


Figure 2: Reaction scheme comparing the electrolyte used in this study and standard thiolate disulfide based redox electrolyte reaction mechanism^[21g]

Thiolate/ disulfide based redox electrolyte have been shown to not absorb in the visible region and have been used in ionic liquids and low volatility electrolytes thus displaying their potential for usage in large area DSC modules. It has been reported by one paper that they are non corrosive to metal substrates but wasn't conclusive enough as it involved a mere dip test of SS and Al strips in the electrolyte solution for a month to check for corrosion pits.^[14]. Therefore we see that these classes of electrolytes show a certain promise to be utilized for inhibition of corrosion of metal surfaces and thus passivates the metal surfaces and requires further investigation. The following figure and table showcase the development so far done in these redox electrolytes^[17].

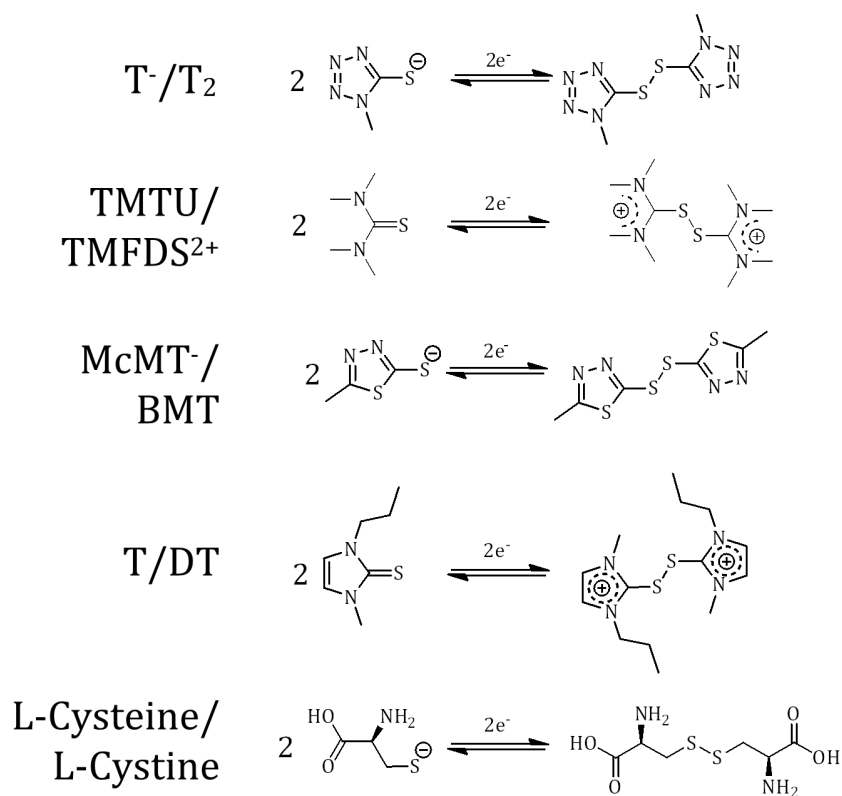


Figure 3: chemical structures of selective published thiolate/disulfide based electrolytes in DSCs.

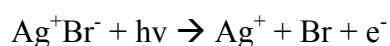
Redox mediator	E_{1/2} (V vs. NHE)	Dye	CE	J_{sc} (mA cm⁻²)	V_{oc} (V)	FF	η (%)
T ₂ /T ⁻	0.49	Z907	Pt	16.18	0.68	0.58	6.44
T ₂ /T ⁻	0.49	Z907	PEDOT	15.90	0.69	0.72	7.90
TMFDS ²⁺ / TMTU	0.55	N3	Carbon	9.45	0.66	0.49	3.10
TMFDS ²⁺ / TMTU	0.55	D131	Carbon	9.16	0.78	0.52	3.88
TMFDS ²⁺ / TMTU	0.55	Z907	Carbon	3.23	0.65	0.66	1.38
BMT/ McMT-	0.16	TH305	Pt	12.20	0.76	0.42	4.00
BMT/ McMT-	0.16	TH305	PEDOT	12.50	0.75	0.65	6.00
DT/T	0.62	N719	Pt	8.20	0.60	0.57	2.80
DT/T	0.62	N719	CoS	9.50	0.65	0.65	3.99
DT/T	0.62	N719	MWCNT	9.80	0.64	0.66	4.12
L-cysteine/ L-cystine	0.45	N719	Pt	17.00	0.72	0.64	7.70

Table 1: Published results of DSCs employing thiolate/disulfide based electrolytes in acetonitrile based solvents measured at one sun simulated AM 1.5 sunlight

2.2 Corrosion Inhibitors:

Although we see that the thiolate disulfide electrolytes do not absorb in the visible spectrum of light, their passivation or corrosion inhibition on metal substrates has not been substantially studied. One of the main approaches to do that would be to look at thiolic/thionic derivatives that have been used in surface treatment of metals. The US

patent 4873139 describes usage of compounds comprising 1-phenyl-1H-tetrazole-5-thiol (PMT) as corrosion inhibitors for silver and copper surfaces^[22]. In the traditional silver based photographic films, the silver halides such as silver bromide, silver iodide etc. are the “grains” that are present as microscopic crystals are used to prepare the photographic films. If we take the example of silver bromide, when it is exposed to light of a particular wavelength, it produces free silver. The schematics of reaction are as follows:



The silver ion then combines with the electron and produces silver atom. The association of silver within the grains produces species such Ag^0 , Ag_4^0 , Ag_4^+ , Ag_2^{2+} , Ag_2^0 . This free silver produced in the exposed silver halide grains is termed *latent image* and is amplified by the developer. The Ag_4^0 free silver is what is produced after the Ag_4^+ is chemically reduced by developers that are then deposited to form the dark section of the film. In the process of reducing the exposed grains, the developer might also reduce the unexposed grains also known as fogging. In order to prevent this, anti fogging agents such as PMT and PMT-Na are used to prevent fogging as they attach to the surface of the unexposed silver halide grains. Thus, this particular compound is widely used in photographic film formulations to control the quantity of unwanted metallic silver which is produced spontaneously with respect to directed image formation (or fog), also as an antihalation agent and for stabilizing images^[23]. The formation of these silver complexes was also postulated by adsorption studies of PMT and $\text{S}_2\text{O}_3^{2-}$ on a silver electrode under electroplating conditions^[24]. In the surface enhanced Raman spectroscopy (SERS)^[25], Bigotto et al. suggested how the PMT adsorbs et al. on to surface of silver metal (figure 4).

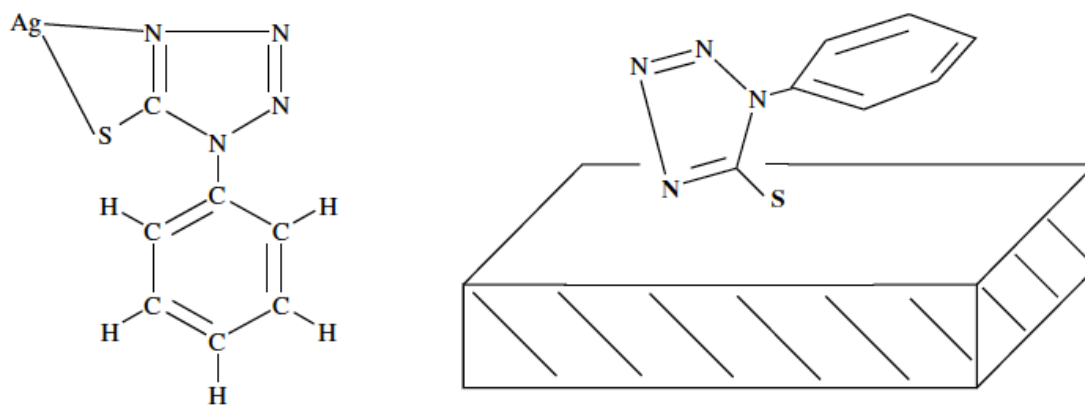


Figure 4: (a) Proposed model in calculation on AgPMTA (b) Proposed model of PMTA on Ag surface. (Taken directly from Bigotto et al)^[25].

Thus we see a promise in using PMT and its derivatives as an alternative to the current iodide-triiodide redox couples and the other class of thiolate disulfide redox couples in order to design new kind of large area DSC modules which would be able to utilize this property of passivating silver grids and thus reduce 1 step in the fabrication of DSC modules.

2.3 Counter Electrodes

One of the major findings of using thiolate disulfide redox couples has been that they work very sluggishly with the conventional platinum counter electrode due to poor catalytic activity in reducing the oxidizing species and thus offering a high charge transfer resistance at the counter electrode-electrolyte interface. It thus limits the device performance and stability. The thiol complexes are known to strongly bind to metal surfaces. This is also a reason why we see a high charge transfer resistance. Alternative materials have been found, leading to increased efficiencies and improved catalytic activities. Mesoporous carbon, PEDOT, PEDOT PSS, metal sulfides, phosphides and carbides have been found to be very efficient^[1c, 20, 21f, 26].

2.4 DSC Module Designs

Modules are units with more than one anode-cathode system connected in series or parallel, comprising cell-to cell seals, often one perimeter seal and two terminal contacts. Electrochemically, a single parallel-connected unit is a “cell”. But from its size and complexity of current collectors, such a unit is referred to as a “module”. The various module designs are shown below:

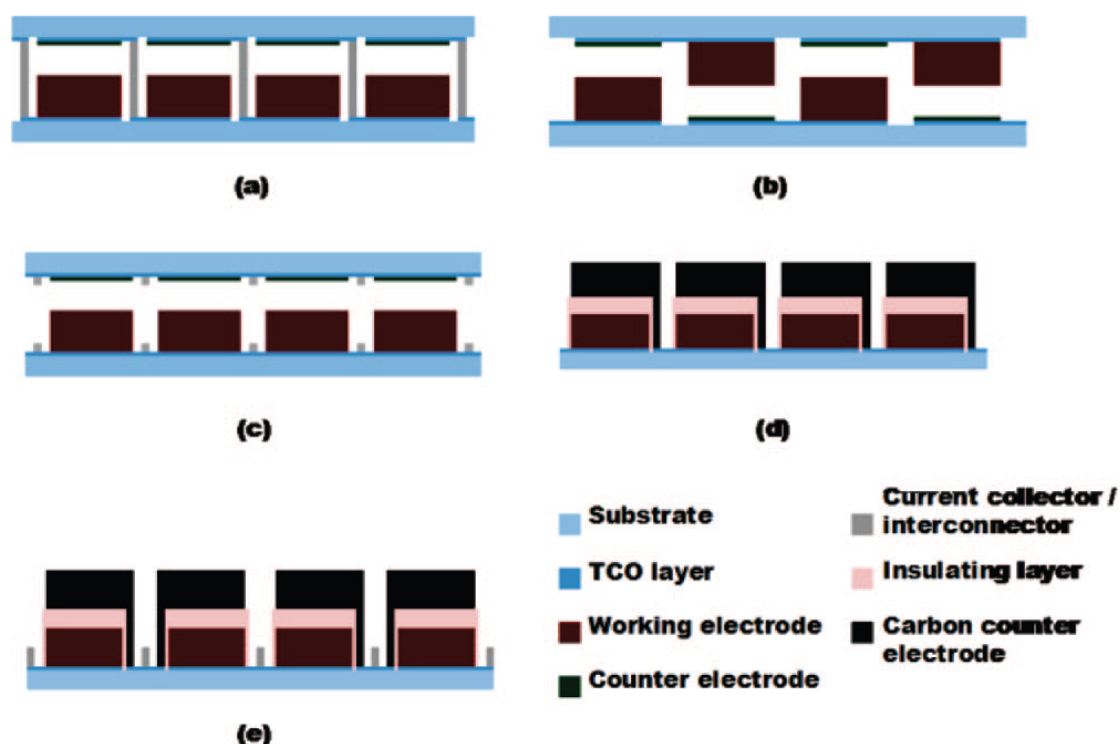


Figure 5: Schematic cross sections of examples of constructions of the five categories of DSC modules: (a) sandwich Z-interconnection; (b) sandwich W-interconnection; (c) sandwich current collection; (d) monolithic serial connection; (e) monolithic current collection. Each module consists of four working and counter electrodes. The proportions of the module layers and substrates are not drawn to scale but have been adjusted to illustrate the device constructions. (Taken from Hagfeldt et al.)^[2]

All the different module designs had one commonality i.e. employing sealants to protect the silver grids. So far, 4 main types of sealants have been investigated for both cells and modules, which are:

- Elastomeric polymers

- Thermoplastic polymers
- Glass frits
- Adhesives (epoxy etc.)

Arakawa et al. reported successful protection of silver grids in a 10 cm x 10 cm p-design module by employing combination of glass frits and polymer over layers.^[10] Glass frits have also been employed successfully by Dyesol in 1995 to protect the silver grids but it required multiple applications, as the frits couldn't be used with rough high conductivity TCOs due to leakage of electrolyte under the glass-TCO seal.^[9]

Thus we see a need to employ alternative strategies to improve upon sealing of DSC modules^[7] or in general remove the need of using sealants to protect silver which can be achieved by employing an alternative electrolyte which gives reasonable efficiencies and passivates the surface of silver grids.

Scope of this thesis

When this research was started, we had seen a slew of research work being done in the field of alternate electrolytes, both metal based and organic based. There was very limited work being done in designing of novel architectures of DSC Modules as the design was getting limited due to corrosive nature of both the conventional iodine based and alternative electrolytes on silver charge collector electrodes. Thus a need was there to study an alternative electrolyte whose chemical structure could assist in preventing corrosion and at the same time act as a redox mediator. This two prong functionality of an electrolyte would certainly assist in attaining newer and novel architectures of DSC modules limiting the need of having epoxy or various other forms of sealants and increase the active area of dye on substrate without the need to protect the silver electrodes.

Also since very limited work was being done in p-DSC and pn-DSC as only iodine and cobalt based electrolytes had shown considerable efficiency in p-DSC and the lack of transparent electrolytes would limit the photon absorption by the dyes in a pn-

DSC solar cell. Thus a need was there to find other alternative electrolytes for p-DSC and pn-DSC, which don't absorb visible light and at the same be able to demonstrate reasonable efficiency at par with iodine/cobalt based electrolytes.

Out of all the aims and roadwork discussed above, in Chapter 3, we were able to demonstrate a suitable thiolate based electrolyte taking advantage of the strong metal-thiolate interaction, designing a smart electrolyte that passivates metal surfaces within the solar cell while also mediating the charge transport and dye regeneration processes, and has shown potential of eliminating complicated and error prone silver protection steps.

We investigated derivatives of 5-mercaptotetrazoles as redox mediator in DSCs and corrosion inhibitors for metal charge collectors employed in large scale DSCs and observed that structural modifications in the 5-mercaptotetrazoles lead to differences in corrosion inhibition properties. Four wire sense measurement and cyclic voltammetry were utilized as characterization tools for characterizing the corrosion inhibition and suppression of recombination by 5-mercaptotetrazoles at the silver metal - electrolyte interface. The results were compared with standard iodine and cobalt based electrolytes. Rate of corrosion was two orders of magnitude lesser for the phenyl based 5-mercaptotetrazole derivative electrolyte compared to standard iodine and cobalt based electrolytes (0.2 nm/hr vs >3600 $\mu\text{m/hr}$ respectively). STM measurements were carried out to characterize the coverage of the silver metal surface by the derivatives of 5-mercaptotetrazoles. Depending on the structure a dense monolayer could be achieved. Small and large area solar cells were fabricated utilizing the 5-mercaptotetrazoles as redox mediator and a proof of principle device achieved reasonable efficiency.

In Chapter 5 we were able to demonstrate application of the above-mentioned electrolyte in a p-type and pn-DSC. The application resulted in an improvement in V_{OC} in p-DSCs compared to the devices based on iodide electrolytes, while maintaining similar J_{SC} (5.3 mA/cm²) values. We also employed the T_{ph} electrolyte in tandem DSCs with film thicknesses optimized for both the T_{ph} and Iodine based electrolytes, we observed that the tandem cells based on the non-corrosive thiolate

electrolyte exhibited similar conversion efficiencies (1.33 %) to those based on iodide electrolytes (1.28%)

References

- [1] a)Y. Liu, J. R. Jennings, M. Parameswaran, Q. Wang, *Energy Environ. Sci.* **2011**, *4*, 564-571; b)Z. Yu, H. Tian, E. Gabrielsson, G. Boschloo, M. Gorlov, L. Sun, L. Kloo, *RSC Adv.* **2012**, *2*, 1083-1087; c)H. Tian, Z. Yu, A. Hagfeldt, L. Kloo, L. Sun, *J. Am. Chem. Soc.* **2011**, *133*, 9413-9422.
- [2] A. Hagfeldt, G. Boschloo, L. Sun, L. Kloo, H. Pettersson, *Chem. Rev.* **2010**, *110*, 6595-6663.
- [3] E. N. Gateway, **Dec 2003**.
- [4] M. A. Green, K. Emery, Y. Hishikawa, W. Warta, E. D. Dunlop, *Prog. Photovolt. Res. Appl.* **2012**, *20*, 12-20.
- [5] C. D. Grant, A. M. Schwartzberg, G. P. Smestad, J. Kowalik, L. M. Tolbert, J. Z. Zhang, *J. Electroanal. Chem.* **2002**, *522*, 40-48.
- [6] a)B. a. G. O'Regan, Michael, *Nature* **1991**, *353*, 737-740; b)A. Yella, H.-W. Lee, H. N. Tsao, C. Yi, A. K. Chandiran, M. K. Nazeeruddin, E. W.-G. Diao, C.-Y. Yeh, S. M. Zakeeruddin, M. Grätzel, *Science* **2011**, *334*, 629-634.
- [7] H. J. S. M. D. M. Brian E. Hardin, *Nature Photonics* **2012**, *6*, 162-169.
- [8] B. Li, L. Wang, B. Kang, P. Wang, Y. Qiu, *Sol. Energy Mater. Sol. Cells* **2006**, *90*, 549-573.
- [9] K. Kalyanasundaram, *Dye-Sensitized Solar Cells*, CRC PRESS, **2010**.
- [10] T. Y. H. Arakawa, S. Agatsuma, T. Sutou, Y. Koishi, in *23rd European Photovoltaic Solar Energy Conference and Exhibition, 1-5 September 2008, VALENCIA, SPAIN, 2008*.
- [11] a)K. Kaneko, H. Akasaka, *Vol. 10738479* (Ed.: L. Threabond Co), EP, **2011**; b)W. J. Lee, E. Ramasamy, D. Y. Lee, J. S. Song, *J. Photochem. Photobiol., A* **2006**, *183*, 133-137; c)H. Pettersson, T. Gruszecki, C. Schnetz, M. Streit, Y. Xu, L. Sun, M. Gorlov, L. Kloo, G. Boschloo, L. Häggman, A. Hagfeldt, *Prog. Photovolt. Res. Appl.* **2010**, *18*, 340-345; d)R. Sastrawan, J. Beier, U. Belledin, S. Hemming, A. Hinsch, R. Kern, C. Vetter, F. M. Petrat, A. Prodi-Schwab, P. Lechner, W. Hoffmann, *Sol. Energy Mater. Sol. Cells* **2006**, *90*, 1680-1691; e)M. Späth, P. M. Sommeling, J. A. M. van Roosmalen, H. J. P. Smit, N. P. G. van der Burg, D. R. Mahieu, N. J. Bakker, J. M. Kroon, *Prog. Photovolt. Res. Appl.* **2003**, *11*, 207-220.

- [12] M. B. H. Desilvestro, S. Tulloch and G. Tullo, *Dye-sensitized solar cells*, EPFL press, Lausanne, **2010**.
- [13] N. C. Mingkui Wang, Livain Breau, Jacques-E. Moser, Robin Humphry-Baker, Benôt Marsan, Shaik M. Zakeeruddin and Michael Grätzel, *Nat. Chem.* **2010**, 2, 385-389.
- [14] D. Li, H. Li, Y. Luo, K. Li, Q. Meng, M. Armand, L. Chen, *Adv. Funct. Mater.* **2010**, 20, 3358-3365.
- [15] a)X. R. Ye, X. Q. Xin, J. J. Zhu, Z. L. Xue, *Appl. Surf. Sci.* **1998**, 135, 307-317; b)D. S. U. S. Kinosky, *Vol. 174837* (Eds.: M. Minnesota, C. Manufacturing), US, **1989**.
- [16] Q. Yu, Y. Wang, Z. Yi, N. Zu, J. Zhang, M. Zhang, P. Wang, *ACS NANO* **2010**, 4, 6032-6038.
- [17] T. Daeneke, Monash University **2012**.
- [18] M. Wang, C. Gratzel, S. M. Zakeeruddin, M. Grätzel, *Energy Environ. Sci.* **2012**.
- [19] M. Wang, N. Chamberland, L. Breau, J. E. Moser, R. Humphry-Baker, B. Marsan, S. M. Zakeeruddin, M. Grätzel, *Nat Chem* **2010**, 2, 385-389.
- [20] M. Wu, Y. Wang, X. Lin, N. Yu, L. Wang, L. Wang, A. Hagfeldt, T. Ma, *Phys. Chem. Chem. Phys.* **2011**, 13, 19298-19301.
- [21] a)L. Wang, M. Wu, Y. Gao, T. Ma, *Appl. Phys. Lett.* **2011**, 98, 221102; b)H. Tian, E. Gabrielsson, Z. Yu, A. Hagfeldt, L. Kloo, L. Sun, *Chem Commun (Camb)* **2011**, 47, 10124-10126; c)H. Tian, X. Jiang, Z. Yu, L. Kloo, A. Hagfeldt, L. Sun, *Angew. Chem. Int. Ed.* **2010**, 49, 7328-7331; d)H. Wu, Z. Lv, Z. Chu, D. Wang, S. Hou, D. Zou, *J. Mater. Chem.* **2011**, 21, 14815; e)M. Cheng, X. Yang, S. Li, X. Wang, L. Sun, *Energy Environ. Sci.* **2012**, 5, 6290; f)D. Noureldine, T. Shoker, M. Musameh, T. H. Ghaddar, *J. Mater. Chem.* **2012**, 22, 862; g)X. Li, Z. Ku, Y. Rong, G. Liu, L. Liu, T. Liu, M. Hu, Y. Yang, H. Wang, M. Xu, P. Xiang, H. Han, *Phys. Chem. Chem. Phys.* **2012**, 14, 14383-14390.
- [22] D. S. Kinosky, (Ed.: USPTO), **1989**.
- [23] a)D. C. Shuman, (Ed.: USPTO), **1993**; b)in ^ Myers, Dr. Drew. "Chemistry of Photography" (HTML). *Cheresources.com. GlobalSpec. Retrieved 2009-01-25*.

- ; c)S. M. Massimo bertoldi, Cristina Soncini, (Ed.: USPTO), **1997**; d)T. M. S. Ikenoue, (Ed.: USPTO), **1976**.
- [24] E. S. Brandt, *Appl. Spectrosc.* **1993**, *47*, 85-93.
- [25] B. Pergolese, A. Bigotto, *J. Raman Spectrosc.* **2002**, *33*, 646-651.
- [26] a)J. S. Jang, D. J. Ham, E. Ramasamy, J. Lee, J. S. Lee, *Chem. Commun.* **2010**, *46*, 8600-8602; b)K. Kitamura, S. Shiratori, *Nanotechnology* **2011**, *22*, 195703; c)A. R. Ko, J.-K. Oh, Y.-W. Lee, S.-B. Han, K.-W. Park, *Mater. Lett.* **2011**, *65*, 2220-2223; d)M. Wu, J. Bai, Y. Wang, A. Wang, X. Lin, L. Wang, Y. Shen, Z. Wang, A. Hagfeldt, T. Ma, *J. Mater. Chem.* **2012**, *22*, 11121; e)M. Wu, X. Lin, A. Hagfeldt, T. Ma, *Angew. Chem. Int. Ed. Engl.* **2011**, *50*, 3520-3524; f)M. Wu, X. Lin, T. Wang, J. Qiu, T. Ma, *Energy Environ. Sci.* **2011**, *4*, 2308; g)M. Wu, X. Lin, Y. Wang, L. Wang, W. Guo, D. Qi, X. Peng, A. Hagfeldt, M. Grätzel, T. Ma, *J. Am. Chem. Soc.* **2012**, *134*, 3419-3428; h)Y. Xiao, J.-Y. Lin, S.-Y. Tai, S.-W. Chou, G. Yue, J. Wu, *J. Mater. Chem.* **2012**, *22*, 19919.

CHAPTER 3

Dual Function Smart Electrolytes For Novel Design of Dye Sensitized Solar Cells: 5-Mercaptotetrazoles as Redox Mediator and Corrosion Repressor

Monash University

Declaration for Thesis Chapter [3]

Declaration by candidate

In the case of Chapter [3], the nature and extent of my contribution to the work was the following:

Nature of contribution	Extent of contribution (%)
All experimental work, preparation of manuscript and editing	60

The following co-authors contributed to the work. If co-authors are students at Monash University, the extent of their contribution in percentage terms must be stated:

Name	Nature of contribution	Extent of contribution (%) for student co-authors only
Torben Daeneke	Experimental design and planning, drafting and editing	N/A
Simon Thompson	Experimental design and planning, drafting and editing	N/A
Julian Lloyd	Design, characterization of STM experiments, drafting and editing	5
Carlos-Andres Palma	Design, characterization of STM experiments, drafting and editing	5
Joachim Reichert	Drafting and editing	N/A
Johannes V. Barth	Drafting and editing	N/A
Leonne Spiccia	Drafting and editing	N/A
Udo Bach	Experimental design and planning, drafting and editing	N/A

The undersigned hereby certify that the above declaration correctly reflects the nature and extent of the candidate's and co-authors' contributions to this work*.

**Candidate's
Signature**

	Date 13.01.16
---	----------------------

**Main
Supervisor's
Signature**

	Date 13.01.16
---	----------------------

Dual-Function Smart Electrolyte for Dye-Sensitized Solar Cells: 5-Mercaptotetrazoles as Redox Mediator and Corrosion Repressor

Rishabh Bhargava,[†] Torben Daeneke,^{§,#} Simon J. Thompson,[†] Julian Lloyd,[†] Carlos-Andres Palma,^{||} Joachim Reichert,^{||} Johannes V. Barth,^{||} Leone Spiccia,[‡] and Udo Bach^{*,†,§,⊥}

[†]Department of Materials Science and Engineering and [‡]School of Chemistry, Monash University, Melbourne, Victoria 3800, Australia

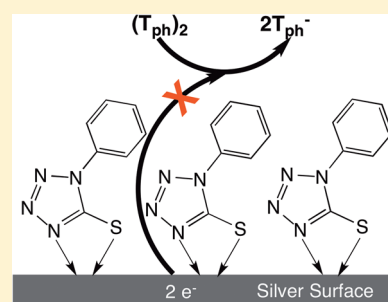
[§]Materials Science and Engineering, CSIRO, Clayton South, Victoria 3169 Australia

^{||}Physik-Department, Technische Universität München, James-Frank-Strasse 1, 85748 Garching, Germany

[⊥]The Melbourne Centre for Nanofabrication, 151 Wellington Road, Clayton South, Victoria 3169, Australia

S Supporting Information

ABSTRACT: Metal charge collectors are an essential component of photovoltaic modules, facilitating charge collection over larger areas. Their application in dye-sensitized solar cells has so far been hampered by two major factors: (1) the redox mediators employed in these photoelectrochemical devices are generally corrosive to metals, and (2) they generally show low overpotentials for their redox reactions on these metal surfaces, which leads to significant recombination losses at the photoanode. Here, a thiolate-based redox mediator, sodium 1-phenyl-1H-5-mercaptotetrazole (T_{ph}), is shown to form self-assembled monolayers on silver electrodes and to act as an effective corrosion protection layer while also exhibiting high overpotentials on these metals at the photoanode. The anticorrosive properties are strongly dependent on the structure of the thiolate. Replacement of the phenyl group in T_{ph} with a methyl substituent accelerates the corrosion process by orders of magnitude. Finally, we demonstrate the applicability of T_{ph} -based electrolytes in a 60 cm² dye-sensitized solar cell comprising unprotected silver charge-collecting electrodes.



INTRODUCTION

Dye-sensitized solar cells (DSCs) have been heralded as a viable alternative technology to standard silicon-based photovoltaics.¹ They have been shown to achieve up to 10% efficiency in modules and up to 13% in small, lab-based devices,^{2–4} making them attractive options for commercialization due to their projected low cost and potential lightweight flexible device architectures.⁵ Iodide-based electrolytes have dominated DSC research for nearly 2 decades,^{6,7} until recently, when several new redox mediators emerged as strong contenders to replace iodine.^{8–10} A major incentive for researching alternative redox mediators is the fact that iodide-based electrolytes are highly corrosive to metals. This complicates the design of large-area DSC modules, since an additional step employing protective sealants, such as epoxy, polymer sealants, and glass frits, is required to protect the metal charge collection electrode (typically silver).^{11–15} These sealants are necessary, since direct contact between the I^-/I_3^- and silver will lead to rapid corrosion of the metal as well as the depletion of triiodide, increasing the series resistance of the device.¹⁶ A second impediment for the application of metallic charge collectors in photoelectrochemical solar cells is the low overpotential exhibited by most redox mediators on these metals, as direct contact of the electrolyte with metallic charge collectors located on the photoanode would result in significant recombination losses across the metal–electrolyte interface. In

2010, Wang et al. introduced an electrolyte based on 5-mercapto-1-methyltetrazole and di-5-(1-methyltetrazole) disulfide [$T_{me}/(T_{me})_2$] achieving efficiencies of up to 6.4%.¹⁷ Following this landmark paper, a number of other thiolate-based electrolytes were studied.^{18–22} These alternative electrolytes have been promising in terms of overall DSC performance, but the repression of corrosive processes in DSCs has not been studied in detail.²³ Thiolates are, however, well-known corrosion inhibitors due to their ability to form strong metal–thiolate bonds.^{24,25} By applying a suitable thiolate/disulfide redox couple in DSCs, we can take advantage of the strong metal–thiolate interaction, designing a smart electrolyte that passivates exposed metal surfaces within the solar cell while also mediating charge transport and dye regeneration processes and potentially eliminating complicated and error prone silver protection steps (see Figure 1).

MATERIALS AND METHODS

Details of the fabrication of the DSCs and devices for corrosion testing are provided in the Supporting Information, as are further experimental details. Materials and chemicals were purchased from commercial suppliers and used as received

Received: May 31, 2015

Revised: July 31, 2015

Published: August 3, 2015

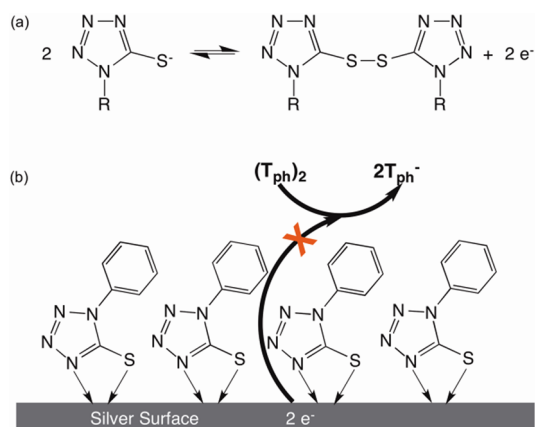


Figure 1. (a) Redox reaction of 5-mercaptotetrazole-based electrolytes (see Figure S2, Supporting Information), wherein R = phenyl for T_{ph} and R = methyl for T_{me} . (b) Schematic diagram showing how T_{ph} binds to the silver surface and how it functions as a passivating layer, blocking the electron flow from silver to the disulfide species in the electrolyte.

unless otherwise stated. The C106 dye solution (for the chemical structure, see Figure S1, Supporting Information) and $T_{me}/(T_{me})_2$ electrolyte were prepared via literature methods.^{17,26,27}

RESULTS AND DISCUSSION

Herein, the surface-passivation properties of electrolytes based on two thiolate redox couples are compared: the archetypal $T_{me}/(T_{me})_2$ redox system as well as $T_{ph}/(T_{ph})_2$. Structurally, these two mediators only differ in the substituent at the 1-position of the 5-mercaptotetrazole ring, featuring a methyl group in the case of T_{me} and a phenyl group in the case of T_{ph} (see Figure 1a). The latter is a well-known corrosion inhibitor for metals^{24,25} and has also found application as an antifogging and toning agent in photography,^{28,29} preventing oxidation of silver particles. Its orientation on the metal surface has previously been studied and a bidentate interaction to metallic silver through the sulfur and nitrogen atom was confirmed by surface-enhanced Raman spectroscopy (Figure 1b).³⁰

The corrosion-inhibiting properties of the electrolytes were investigated by exposing a silver film to the electrolyte while periodically measuring its conductivity, which is proportional to the thickness of the silver layer. Figure 2a,b shows the change in conductance over time for a 100–150 nm thick silver film when exposed to various commonly employed electrolytes. Exposure to a standard iodide (I^-/I_3^-) electrolyte resulted in a total loss of conductivity within less than 1 min (corrosion rate: >3 nm/s (10.8 $\mu\text{m}/\text{h}$). Surprisingly, exposure to a $[\text{Co}(\text{bpy})_3]^{2+/3+}$ electrolyte resulted in complete corrosion of the silver layer in less than 2 min [corrosion rate >1 nm/s (3.6 $\mu\text{m}/\text{h}$)]. This is conflicting with the general view that simple transition-metal-based complexes, such as $[\text{Co}(\text{bpy})_3]^{2+/3+}$, are significantly less corrosive than iodide-based electrolytes.³¹

A visual inspection of the sample revealed that the silver film had completely dissolved. The investigation of an electrolyte based on the $T_{me}/(T_{me})_2$ thiolate/disulfide redox couple originally introduced by Wang et al. showed a slower degradation rate than the iodide- and cobalt-based electrolytes (Figure 2b, corrosion rate 20 nm/h). The conductance of the silver layer, however, was gradually reduced to zero and the exposed silver film had completely corroded within 3–4 h.

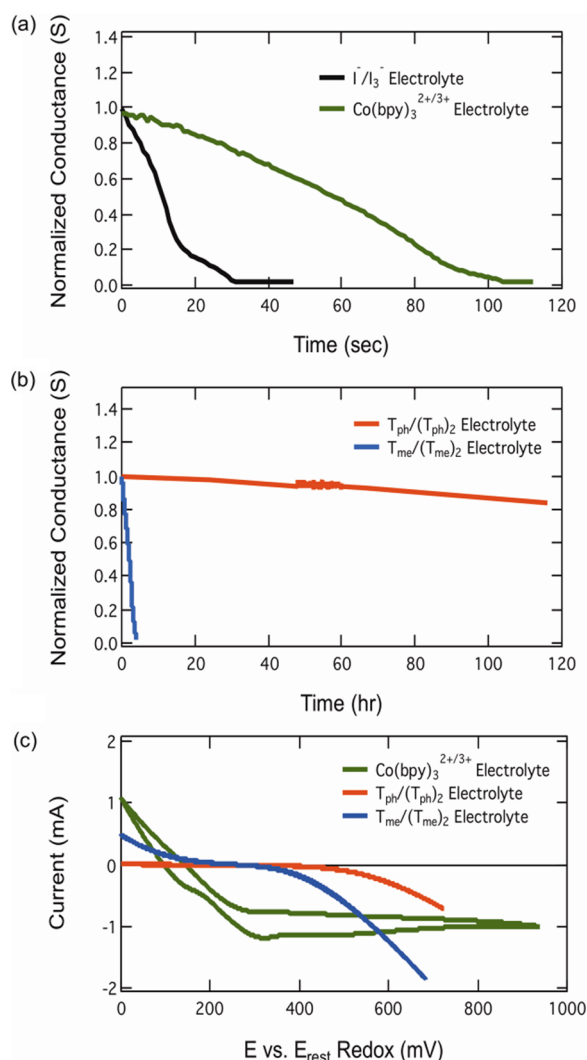


Figure 2. (a and b) Time-dependent conductance of a 100–150 nm thick silver film upon exposure to (a) I^-/I_3^- (black) and $[\text{Co}(\text{bpy})_3]^{2+/3+}$ (green) electrolytes and (b) $T_{me}/(T_{me})_2$ (blue) and $T_{ph}/(T_{ph})_2$ (red) electrolytes. (c) Cyclic voltammogram of $\text{Co}(\text{bpy})_3^{2+/3+}$ (green), $T_{me}/(T_{me})_2$ (blue), and $T_{ph}/(T_{ph})_2$ (red) electrolytes on printed 0.49 cm^2 , 12 μm thick silver electrodes on FTO glass, measured in a three-electrode configuration using a Pt wire as a counter electrode and an Ag/AgNO_3 reference electrode. The measured current is plotted against the applied anodic potential with reference to the rest potential of each electrolyte, showing the relevant potential range of each cyclic voltammogram for device operation. The scan rate was 20 mV/s. Further details are provided in the Supporting Information.

Despite the strong structural similarity between T_{me} and T_{ph} , substantial differences in their corrosive properties were observed. Over a period of 120 h, the thickness of the silver layer exposed to a $T_{ph}/(T_{ph})_2$ electrolyte was only reduced by 20% (corrosion rate 0.2 nm/h). The equivalent reduction in conductivity for the $T_{me}/(T_{me})_2$ electrolyte was already observed after 1 h, indicating a difference in silver etching rates of about 2 orders of magnitude between the two thiolates, and highlighting the important influence of the molecular structure on the electrochemical properties.

Cyclic voltammetry was utilized to characterize the silver metal/electrolyte interface. Figure 2c shows the anodic scans of $\text{Co}(\text{bpy})_3^{2+/3+}$, $T_{me}/(T_{me})_2$, and $T_{ph}/(T_{ph})_2$ -based electrolytes

with reference to their rest potential (-0.06 , -0.317 , and -0.276 V, respectively, vs Ag/AgNO_3). The vertex potential was chosen to be slightly larger than typically observed open circuit potentials for dye-sensitized solar cells employing the respective electrolyte (700 – 900 mV). In the case of the cobalt-based electrolyte, a positive current was observed at low applied bias potentials (0 – 200 mV). This current can be attributed to the corrosion of the silver film. At higher applied bias potentials, a negative current is observed that is diffusion-limited for potentials greater than 300 mV. The observation of a diffusion limit indicates charge transport limitations in the electrolyte. Negative currents represent the transfer of electrons to the oxidized redox mediator in the electrolyte. In a solar cell, this would lead to recombination losses, since charge collection electrodes on the photoanode would facilitate the charge transfer of the photoinjected electrons to the oxidized redox mediator.

In the case of $T_{\text{me}}/(T_{\text{me}})_2$, a positive current can be observed for low applied potentials (<250 mV), indicating the corrosion of the silver metal. At higher applied potentials (>250 mV), a negative current is observed, which can be attributed to the reduction of the disulfide on the silver surface. No diffusion limitation was observed, highlighting the good conductivity of the $T_{\text{me}}/(T_{\text{me}})_2$ electrolyte. A significant current is observed at comparatively low potentials of 400 mV, making the $T_{\text{me}}/(T_{\text{me}})_2$ electrolyte a poor choice for the use in large-scale dye-sensitized solar cells with unprotected silver charge collectors on the photoanode. The $T_{\text{ph}}/(T_{\text{ph}})_2$ electrolyte on the other hand shows a diodelike behavior. No positive current is observed, which is in good agreement with the observed low metal corrosion rates for this electrolyte. The negative current onset occurs at an applied voltage between 450 and 500 mV, with significant currents of over $250 \mu\text{A}$ being observed for potentials above 600 mV. While this may lead to some recombination losses under operational conditions, we can expect to maintain high open circuit voltages for a large DSC module with unprotected silver charge collectors. The results highlight that the $T_{\text{ph}}/(T_{\text{ph}})_2$ electrolyte can repress the corrosion of the silver metal while also forming a nonohmic contact with the metal that provides a large overpotential for the recombination between the photoinjected electron and the oxidized redox mediator via the metal interface.

Scanning tunneling microscopy (STM) investigations were conducted to gain insight into the surface structure of the self-assembled monolayers formed on $\text{Ag}(111)$ single-crystal surfaces upon exposure to saturated solutions of T_{ph} and T_{me} . The STM images of the freshly cleaned $\text{Ag}(111)$ surface (see Figure 3a,b) show clearly visible, sharp edges, which indicate the absence of adsorbed molecular species at this stage and atomically flat terraces, as shown in Figure 3b. After exposing the surface to a T_{ph} solution, the STM images indicate monolayer coverage of the silver surface by T_{ph} (Figure 3c). This is evidenced by the still clearly visible, now rougher step edges of the underlying surface as well as the rise of substructures and small defects on the surface planes. In the high-resolution STM images (Figure 3d), densely packed molecular-sized substructures are visible on the surface.

Changing from T_{ph} to T_{me} results in a markedly different morphology (Figure 3e,f). The greater surface roughness for T_{me} suggests the formation of a multilayer assembly or interfacial mass transport of Ag surface atoms. This is further supported by the lack of clearly resolved step edges of the underlying surface and the absence of molecular-sized features

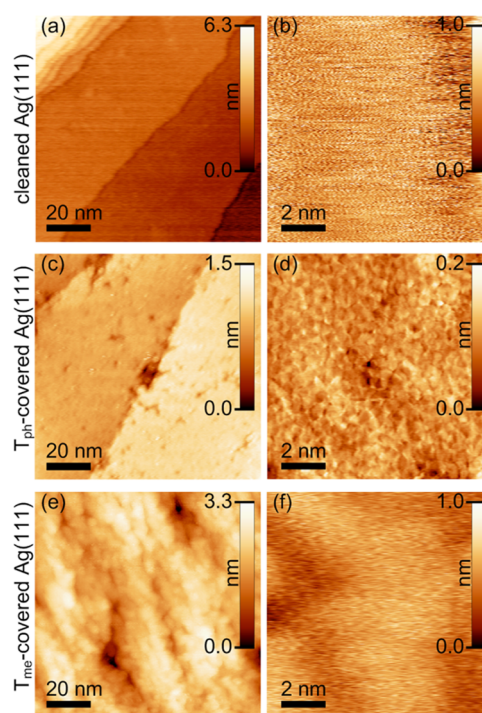


Figure 3. Scanning tunneling microscopy images of $\text{Ag}(111)$ surfaces after different preparations: (a and b) Ar^+ -cleaned $\text{Ag}(111)$ surface prior to thiolate absorption measured in air, (c and d) $\text{Ag}(111)$ surfaces after exposure to a 0.4 M T_{ph} solution in dimethylformamide (DMF) for 1 h measured in trichlorobenzene (TCB), and (e and f) $\text{Ag}(111)$ surfaces after exposure to a 0.4 M T_{me} solution in DMF for 1 h recorded in TCB and air, respectively. Further information on STM testing conditions is provided in the [Supporting Information](#).

in the high-resolution images. Thus, the self-assembly properties of thiolates on silver surface are strongly governed by their molecular structure, leading to a densely packed layer formation at the interface in the case of T_{ph} .

Dye-sensitized solar cells were fabricated to investigate the performance of DSCs applying the $T_{\text{ph}}/(T_{\text{ph}})_2^-$ and $T_{\text{me}}/(T_{\text{me}})_2^-$ -based electrolytes in conjunction with the ruthenium-based sensitizer C106 (Figure S1, [Supporting Information](#)). Small test cells with an area of 0.16 cm^2 were initially studied at simulated 1000 W m^{-2} AM1.5G irradiation. The devices show very similar performances and efficiencies in the range of 4.4% , with both electrolytes achieving high photocurrent densities above 12 mA cm^{-2} and photovoltages around 650 mV (see Figures S3 and S4 and Tables S1 and S2, [Supporting Information](#)). The efficiencies were, however, limited by a comparatively low fill factor of about 0.5 for both redox mediators. Printed carbon counter electrodes were utilized in this study due to scalability considerations. Other novel catalysts have recently been reported that could help to improve the fill factor, opening an avenue for future device performance improvements provided they can be translated to large-scale devices.^{32,33} The photovoltages were limited by the low rest potentials of the $T_{\text{ph}}/(T_{\text{ph}})_2^-$ and $T_{\text{me}}/(T_{\text{me}})_2^-$ -based electrolytes. Molecular engineering targeted at adjusting the redox potential of the mediator while preserving the formation of the self-assembled monolayer is expected to increase the efficiency of the devices further.^{18,19,34}

Proof-of-concept large-area DSCs, with a 60 cm^2 active surface area, were fabricated in a second part of this study (Figure S3b and Table S1, [Supporting Information](#)). Silver

charge-collecting electrodes with a width of 1 mm and thickness of 13 μm were printed on FTO glass with a center-to-center spacing of 6 mm (see Figure S5, Supporting Information). Typically, whenever metal collecting electrodes had previously been integrated into DSCs they needed to be thoroughly protected from any electrolyte contact to avoid corrosion by depositing a Surlyn, glass, or epoxy-based barrier around the metal electrode. This imposes additional space requirements, reducing the fill ratio (FR) of the active device surface area to actual module surface area. In our case the unpatterned 9.1×8.6 cm TiO_2 film was printed directly onto the FTO electrode with no additional protection layer. Consequently, the fill ratio of this device, simply defined by the actual printed surface areas of TiO_2 (A_{TiO_2}) and silver (A_{Ag}) according to $\text{FR} = (A_{\text{TiO}_2} - A_{\text{Ag}})/A_{\text{TiO}_2}$, was 78%, which was 27% higher compared to a standard module device. The large-area DSC yielded a short circuit current density (J_{SC}) of 5.35 mA cm^{-2} and a V_{OC} of 600 mV. The lower voltage can be rationalized by the recombination losses at the metal/electrolyte interface at high potentials, as seen in Figure 2c. While this leads to an approximate voltage loss of 10%, the benefit of a module with an increased fill ratio outweighs the sacrifice. Future optimization of the molecular design of the redox mediator or the choice of another charge collection metal may lead to higher overpotentials for the recombination reaction, allowing this limitation to be overcome entirely, opening an avenue for future research. The fill factor of 0.41 was only slightly reduced when compared to the small-area test cell. The overall conversion efficiency was 1.33%. For comparison, a large-area DSC fabricated without charge collection electrodes exhibited a fill factor of only 0.24, which is typical for solar cells limited by their series resistance. The short-circuit current density was limited by the resistivity of the FTO substrate to 0.65 mA cm^{-2} , highlighting the need for charge collection metal electrodes for nonseries connected large-area DSCs. Optimization of the device design should lead to better conversion efficiencies and improve the scalability of the efficiency from small- to large-area devices, especially with regard to the photocurrent density.

The long-term stability of the module was, however, not satisfactory, and the device degraded within several days (data not shown). The efficiency decline was partially attributed to device-sealing issues and to the loss of the oxidized redox couple, along with the slow oxidation of silver. While molecular design enabled the reaction rate to be reduced by 2 orders of magnitude, allowing the fabrication of proof of principle devices, further improvements are necessary for commercial application of the developed concepts. Modules with improved efficiency and long-term stability should be feasible following the here-demonstrated strategies, provided the molecular design is improved with respect to the formation of the passivating monolayer.

CONCLUSION

In conclusion, the surface-passivating properties of 5-mercaptotetrazoles were found to be highly dependent on their chemical structure. A comparison of two 5-mercaptotetrazole derivatives showed that simple substitution of a methyl group with a phenyl group fundamentally changes the self-assembly properties and accordingly leads to an improved ability to form a protective monolayer on metal electrodes. As a result, we show that 5-mercaptotetrazoles can be used as a dual

function agent in DSCs: first, as a surface-passivating agent, impeding corrosion and recombination across the metal–electrolyte interface, and, second, as the redox mediators, accomplishing quantitative dye regeneration. Thermodynamically, many DSC mediators exhibit electrochemical potentials suitable not only to ensure quantitative dye regeneration but also to spontaneously drive the corrosion of metals such as silver. The latter is a significant impediment toward the application of metals as charge collection electrodes. Due to their electrochemical potential, 5-mercaptotetrazoles are capable of oxidizing silver electrodes, yet in this study we show that their strong interaction with silver surfaces results in the formation of a self-assembled monolayer, impeding their own redox reactions. The surface passivation has two desirable consequences: (1) a strong suppression of silver corrosion, and (2) a high overpotential for the reduction of the corresponding disulfides of 5-mercaptotetrazole at the silver electrode of the photoanode. The latter results in the suppression of the recombination reaction between the separated charges via the Ag metal surface. Both the suppression of the corrosion process and the interfacial recombination losses are necessities for the application of the redox electrolyte in direct contact with the charge-collecting electrode. This allowed us to fabricate a fully printable prototype device with an improved fill ratio, since no protective layers had to be deposited on top of the charge collection electrodes. While the corrosion rates observed for T_{ph} were exceptionally low, the actual corrosion process itself over the period of several years would likely still be problematic for the application of unprotected silver electrodes in DSCs. Nevertheless, the strong correlation revealed here between the molecular structure of the two 5-mercaptotetrazoles and their surface passivation properties provides a strong stimulus for the design and development of the next generation of thiolate-based redox mediators with further improved self-assembly and corrosion-protection properties. Stability issues will need to be addressed for thiol-based redox mediators. A possible approach could involve utilizing the thiol-based mediator in combination with a stable redox couple, taking advantage of the corrosion-suppressing properties that have been identified in this work.

The developed concepts may find further application in metal halide–organic perovskite-based solar cells, which have received significant research attention due to their high efficiencies of up to 20%. During the fabrication of these devices, highly corrosive halide solutions are deposited on the substrate, which would be detrimental for any metal charge collectors. Passivation of these metal charge collectors using self-assembled T_{ph} monolayers either prior to or during the deposition of the light-absorbing perovskite layer could lead to efficient, large-area modules with high fill ratios. Since the halide-containing solution is completely dried during the production process, a more favorable device stability profile may be anticipated for these devices.

ASSOCIATED CONTENT

Supporting Information

The Supporting Information is available free of charge on the ACS Publications website at DOI: 10.1021/acs.jpcc.5b05195.

Details on the used chemicals and materials and device fabrication and characterization, as well as chemical structures, representative J – V curves, tabulated J – V data, large area device data, and photographs of the large area devices (PDF)

AUTHOR INFORMATION

Corresponding Author

Present Address

#School of Electrical and Computer Engineering, RMIT University, Melbourne, Victoria 3001, Australia.

Author Contributions

The paper was written through contributions of all authors. All authors have given approval to the final version of the manuscript.

Notes

The authors declare no competing financial interest.

ACKNOWLEDGMENTS

This program has been supported by CSIRO through the OCE Science Leader program and the Australian Government through the Australian Renewable Energy Agency (ARENA) and the Australian Solar Institute. Further financial support has been made available by the Victorian Government through the DSDBI and VSA programs. We acknowledge financial support from the Victorian State Government Department of Primary Industry, Bluescope Steel, Innovia Films, Innovia Security, and Bosch (Victorian Organic Solar Cells Consortium). This work was performed in part at the Melbourne Centre for Nanofabrication, an initiative partly funded by the Australian National Fabrication Facility (ANFF), the Commonwealth of Australia, and the Victorian Government. The ARC is acknowledged for providing support through an ARF fellowship (U. B.). The work was supported by the Munich Centre for Advanced Photonics (MAP) funded by the German Research Foundation (DFG) via the German Excellence Initiative.

REFERENCES

(1) Toyoda, T.; Sano, T.; Nakajima, J.; Doi, S.; Fukumoto, S.; Ito, A.; Tohyama, T.; Yoshida, M.; Kanagawa, T.; Motohiro, T.; et al. Outdoor performance of large scale DSC modules. *J. Photochem. Photobiol., A* **2004**, *164*, 203–207.

(2) Baxter, J. B. Commercialization of dye sensitized solar cells: Present status and future research needs to improve efficiency, stability, and manufacturing. *J. Vac. Sci. Technol., A* **2012**, *30*, 020801.

(3) Miettunen, K.; Halme, J.; Lund, P. Metallic and plastic dye solar cells. *Wiley Interdisciplinary Reviews: Energy and Environment* **2013**, *2*, 104–120.

(4) Green, M. A.; Emery, K.; Hishikawa, Y.; Warta, W.; Dunlop, E. D. Solar cell efficiency tables (version 42). *Prog. Photovoltaics* **2013**, *21*, 1–11.

(5) Ikegami, M.; Suzuki, J.; Teshima, K.; Kawaraya, M.; Miyasaka, T. Improvement in durability of flexible plastic dye-sensitized solar cell modules. *Sol. Energy Mater. Sol. Cells* **2009**, *93*, 836–839.

(6) O'Regan, B.; Grätzel, M. A low-cost, high-efficiency solar cell based on dye-sensitized colloidal TiO₂ films. *Nature* **1991**, *353*, 737–740.

(7) Hagfeldt, A.; Boschloo, G.; Sun, L.; Kloo, L.; Pettersson, H. Dye-sensitized solar cells. *Chem. Rev.* **2010**, *110*, 6595–6663.

(8) Yella, A.; Lee, H.-W.; Tsao, H. N.; Yi, C.; Chandiran, A. K.; Nazeeruddin, M. K.; Diau, E. W.-G.; Yeh, C.-Y.; Zakeeruddin, S. M.; Grätzel, M. Porphyrin-sensitized solar cells with cobalt (II/III)-based redox electrolyte exceed 12% efficiency. *Science* **2011**, *334*, 629–634.

(9) Daeneke, T.; Kwon, T.-H.; Holmes, A. B.; Duffy, N. W.; Bach, U.; Spiccia, L. High-efficiency dye-sensitized solar cells with ferrocene-based electrolytes. *Nat. Chem.* **2011**, *3*, 211–215.

(10) Mathew, S.; Yella, A.; Gao, P.; Humphry-Baker, R.; Curchod, B. F.; Ashari-Astani, N.; Tavernelli, I.; Rothlisberger, U.; Nazeeruddin, M.

K.; Grätzel, M. Dye-sensitized solar cells with 13% efficiency achieved through the molecular engineering of porphyrin sensitizers. *Nat. Chem.* **2014**, *6*, 242–247.

(11) Kaneko, K.; Akasaka, H. Sealing agent composition for dye-sensitized solar cell. Patent EP 2395596 A4, 2011.

(12) Lee, W. J.; Ramasamy, E.; Lee, D. Y.; Song, J. S. Glass frit overcoated silver grid lines for nano-crystalline dye sensitized solar cells. *J. Photochem. Photobiol., A* **2006**, *183*, 133–137.

(13) Pettersson, H.; Gruszecki, T.; Schnetz, C.; Streit, M.; Xu, Y.; Sun, L.; Gorlov, M.; Kloo, L.; Boschloo, G.; Häggman, L.; et al. Parallel-connected monolithic dye-sensitized solar modules. *Prog. Photovoltaics* **2010**, *18*, 340–345.

(14) Sastrawan, R.; Beier, J.; Belledin, U.; Hemming, S.; Hirsch, A.; Kern, R.; Vetter, C.; Petrat, F. M.; Prodi-Schwab, A.; Lechner, P.; et al. A glass frit-sealed dye solar cell module with integrated series connections. *Sol. Energy Mater. Sol. Cells* **2006**, *90*, 1680–1691.

(15) Späth, M.; Sommeling, P. M.; van Roosmalen, J. A. M.; Smit, H. J. P.; van der Burg, N. P. G.; Mahieu, D. R.; Bakker, N. J.; Kroon, J. M. Reproducible manufacturing of dye-sensitized solar cells on a semi-automated baseline. *Prog. Photovoltaics* **2003**, *11*, 207–220.

(16) Kalyanasundaram, K. *Dye-Sensitized Solar Cells*, 1st ed.; EPFL Press: Lausanne, Switzerland, 2010; p 320.

(17) Wang, M.; Chamberland, N.; Breau, L.; Moser, J.-E.; Humphry-Baker, R.; Marsan, B.; Zakeeruddin, S. M.; Grätzel, M. An organic redox electrolyte to rival triiodide/iodide in dye-sensitized solar cells. *Nat. Chem.* **2010**, *2*, 385–389.

(18) Tian, H.; Jiang, X.; Yu, Z.; Kloo, L.; Hagfeldt, A.; Sun, L. Efficient organic-dye-sensitized solar cells based on an iodine-free electrolyte. *Angew. Chem., Int. Ed.* **2010**, *49*, 7328–7331.

(19) Cheng, M.; Yang, X.; Li, S.; Wang, X.; Sun, L. Efficient dye-sensitized solar cells based on an iodine-free electrolyte using L-cysteine/L-cystine as a redox couple. *Energy Environ. Sci.* **2012**, *5*, 6290–6293.

(20) Liu, Y.; Jennings, J. R.; Parameswaran, M.; Wang, Q. An organic redox mediator for dye-sensitized solar cells with near unity quantum efficiency. *Energy Environ. Sci.* **2011**, *4*, 564–571.

(21) Yu, Z.; Tian, H.; Gabrielsson, E.; Boschloo, G.; Gorlov, M.; Sun, L.; Kloo, L. Tetrathiafulvalene as a one-electron iodine-free organic redox mediator in electrolytes for dye-sensitized solar cells. *RSC Adv.* **2012**, *2*, 1083–1087.

(22) Tian, H.; Yu, Z.; Hagfeldt, A.; Kloo, L.; Sun, L. Organic redox couples and organic counter electrode for efficient organic dye-sensitized solar cells. *J. Am. Chem. Soc.* **2011**, *133*, 9413–22.

(23) Li, D.; Li, H.; Luo, Y.; Li, K.; Meng, Q.; Armand, M.; Chen, L. Non-corrosive, non-absorbing organic redox couple for dye-sensitized solar cells. *Adv. Funct. Mater.* **2010**, *20*, 3358–3365.

(24) Ye, X. R.; Xin, X. Q.; Zhu, J. J.; Xue, Z. L. Coordination compound films of 1-phenyl-5-mercaptotetrazole on copper surface. *Appl. Surf. Sci.* **1998**, *135*, 307–317.

(25) Kinosky, D. S. Corrosion resistant silver and copper surfaces. U.S. Patent 4873139, 1989.

(26) Cao, Y.; Bai, Y.; Yu, Q.; Cheng, Y.; Liu, S.; Shi, D.; Gao, F.; Wang, P. Dye-sensitized solar cells with a high absorptivity ruthenium sensitizer featuring a 2-(hexylthio)thiophene conjugated bipyridine. *J. Phys. Chem. C* **2009**, *113*, 6290–6297.

(27) Thompson, S. J.; Duffy, N. W.; Bach, U.; Cheng, Y.-B. On the role of the spacer layer in monolithic dye-sensitized solar cells. *J. Phys. Chem. C* **2010**, *114*, 2365–2369.

(28) Brandt, E. S. Selective enhanced raman scattering from an oxacarbocyanine dye and 1-phenyl-5-mercaptotetrazole adsorbed to silver and silver halide surfaces in photographic films. *Appl. Spectrosc.* **1993**, *47*, 85–93.

(29) Rott, A.; Weyde, E. *Photographic Silver Halide Diffusion Processes*; Focal Press: London, 1972.

(30) Pergolesi, B.; Bigotto, A. SERS studies of the adsorption of 1-phenyl-5-mercaptotetrazole on silver sols. *J. Raman Spectrosc.* **2002**, *33*, 646–651.

(31) Cazzanti, S.; Caramori, S.; Argazzi, R.; Elliott, C. M.; Bignozzi, C. A. Efficient non-corrosive electron-transfer mediator mixtures for dye-sensitized solar cells. *J. Am. Chem. Soc.* **2006**, *128*, 9996–9997.

(32) Wu, M.; Lin, X.; Wang, Y.; Wang, L.; Guo, W.; Qi, D.; Peng, X.; Hagfeldt, A.; Grätzel, M.; Ma, T. Economical Pt-free catalysts for counter electrodes of dye-sensitized solar cells. *J. Am. Chem. Soc.* **2012**, *134*, 3419–28.

(33) Fang, X.; Ma, T.; Akiyama, M.; Guan, G.; Tsunematsu, S.; Abe, E. Flexible counter electrodes based on metal sheet and polymer film for dye-sensitized solar cells. *Thin Solid Films* **2005**, *472*, 242–245.

(34) Sun, Z.; Liang, M.; Chen, J. Kinetics of iodine-free redox shuttles in dye-sensitized solar cells: interfacial recombination and dye regeneration. *Acc. Chem. Res.* **2015**, *48*, 1541–1550.

Supporting Information to: Dual-Function Smart Electrolyte for Dye-Sensitized Solar Cells: 5-Mercaptotetrazoles as Redox Mediator and Corrosion Repressor

Rishabh Bhargava^a, Torben Daeneke^b, Simon Thompson^a, Julian Lloyd^a, Carlos-Andres Palma^c, Joachim Reichert^c, Johannes V. Barth^c, Leone Spiccia^d and Udo Bach^{a,b,e*}

[a] Rishabh Bhargava, Dr. Simon Thompson, Julian Lloyd and Prof. Udo Bach, Department of Materials Science and Engineering, Monash University Victoria 3800, Australia

[b] Dr. Torben Daeneke and Prof. Udo Bach, CSIRO Materials Science and Engineering Clayton South, Victoria 3169 Australia

[c] Dr. Carlos-Andres Palma, Dr. Joachim Reichert and Dr. Johannes V. Barth, Physik-Department Technische Universität München James-Franck-Str. 1, 85748 Garching

[d] Prof. Leone Spiccia, School of Chemistry Monash University Victoria 3800, Australia

[e] Prof. Udo Bach, The Melbourne Centre for Nanofabrication 151 Wellington Road, Clayton South, Victoria 3169, Australia

Materials & Reagents:

The following chemicals and solvents were purchased from Sigma-Aldrich: titanium diisopropoxide bis(acetylacetonate) (TAA) 7.5% in isopropanol solution, acetonitrile, N,N dimethyl formamide (DMF), Sodium 1-phenyl-1-H-tetrazole-5-thiolate, 5,5'-dithiobis(1-phenyl-1-H-tetrazole), 4-tert-butylpyridine (tBp), 10 μm \emptyset graphite powder and 20 nm \emptyset zirconia powder. Lithium bis(trifluoromethanesulfonylimide) (LiTFSI) was purchased from IoLeTec. Chenodeoxycholic acid was purchased from Acros. The C106 dye was purchased from Organica and the dye solution was prepared as per literature^[1]. The FTO glass substrates ($8\Omega/\square$, 3 mm thick) were purchased from Dyesol. The titania pastes were purchased from JGC C&C Japan (CCIC PST-18NR, CCIC PST-400C). The silver paste was purchased from DuPont. 250 nm particle carbon black was purchased from Cabot. P25 titania powder was purchased from Degussa. Zirconia 300 nm particles powder (TZ-3Y) was purchased from TOSOH. Surlyn sheets were purchased from Solaronix. The carbon & zirconia pastes were prepared using the method given by Thompson et al^[2]. Sodium 5-mercapto-1-methyltetrazole (T_{me}) & di-5- (1-methyltetrazole) disulfide ($(T_{\text{me}})_2$) were prepared as reported in the literature^[3]. The I^-/I_3^- electrolyte was prepared as per literature^[4]. The cobalt complexes, tris(2,2'-bipyridine)cobalt(II) bis(trifluoromethanesulfonyl)imide, $[\text{Co}(\text{bpy})_3](\text{TFSI})_2$ and $[\text{Co}(\text{bpy})_3](\text{TFSI})_3$ were prepared following literature methods^[5].

Small Area Cells:

TiO₂ working electrode preparation:

The FTO glass substrates were cleaned in an ultrasonic bath for 10 min in 5% Helmanex in water solution followed by rinsing with reverse osmosis (R.O.) water and a further sonication step (10 min) in ethanol. These substrates were then coated with a dense TiO₂ blocking layer by spray pyrolysis at 450°C by using a titanium diisopropoxide bis(acetylacetonate) (TAA) 7.5% in isopropanol solution. Titania pastes were screen printed on FTO glass substrates by using a commercial semi automatic screen printer, with a 90T mesh. One print was found to deposit a 2 μm thick titania layer. Subsequent layers were deposited to reach a 6 μm film thickness of the transparent paste CCIC PST-18NR (18 nm Ø) and a 6 μm thickness of the scattering film CCIC PST- 400C (400 nm Ø). The films were sintered using a hot plate at 150°C for 10 minutes, at 325°C for 5 minutes, at 375°C for 5 minutes, at 450°C for 30 minutes and finally at 500°C for 15 minutes. After cooling, these substrates underwent a TiCl₄ post treatment, using a 0.05M TiCl₄ solution prepared by diluting a 2M aqueous stock solution with R.O. water. The films were immersed in 150 ml of 0.05M TiCl₄ solution and heated in an oven at 70°C for 30 minutes. After that, they were washed with ethanol and left to dry and stored until use. The printed transparent and scattering titania film thickness was measured to be 12 μm, using a Veeco Dektak 6m stylus profilometer. The dimensions of the printed films were 4 mm x 4 mm (area 0.16 cm²).

Before soaking the films in the dye solution, the working electrodes were reheated at 500°C for 30 minutes using a Leister heat gun to remove absorbed water and organics from the titania surface. After cooling to 80°C, the films were immersed into the dye bath. Dye adsorption was achieved from a 0.3mM C106 dye solution (see Figure S1) in DMF containing 2mM chenodeoxycholic acid, used as a co-adsorbent^[1]. After 20 hours of dye uptake, the films were rinsed in DMF followed by acetonitrile and assembled to DSCs.

Carbon counter electrode preparation:

The carbon paste was prepared using the method given by Thompson et al.^[2] using a solids ratio of 60% 10 μm Ø graphite, 15% 250 nm Ø carbon black and 25% P25 titania. The carbon paste was screen printed on pre drilled FTO glass substrate using a commercial semi automatic screen printer, with an 18T mesh. One print was found to deposit a 10 to 12 μm thick carbon layer. The films were sintered on a hot plate at 400°C for 30 minutes. After cooling, they were stored until use. Prior to device fabrication they were reheated to 400°C for 30 minutes to remove absorbed water and volatile organics from the carbon surface. After cooling below 200°C, they were removed, rapidly cooled and used immediately. The printed carbon film thickness was 20 μm, measured using a Veeco Dektak 6m stylus profilometer. The dimensions of the printed films were 4 mm x 4 mm (area 0.16 cm²)

Preparation of electrolytes:

- a) The optimized T_{ph}/(T_{ph})₂ electrolyte contained 0.40 M of the reduced species (sodium 1-phenyl-1-H-tetrazole-5-thiolate), 0.30 M of the oxidized species (5,5'-dithiobis(1-phenyl-1-H-tetrazole)), 0.05 M

lithium bis(trifluoromethanesulfonylimide) (LiTFSI) and 0.50 M of 4-tert-butylpyridine (tBp) in N, N'-dimethylformamide (DMF). The concentration of the reduced & oxidized species were 0.4M and 0.1M, respectively, when acetonitrile was used as the solvent, since the concentration of 0.1M of the oxidized species (T_{ph}^+) in acetonitrile was approaching the solubility limit.

- b) Sodium 5-mercapto-1-methyltetrazole (T_{me}) and di-5-(1-methyltetrazole)disulfide ($(T_{me})_2$) were prepared as reported in the literature^[3]. The concentration of the reduced and oxidized species were equal to those described in a) (0.4M/0.3M in DMF and 0.4M/0.1M in acetonitrile) the remaining concentrations of the additives were equal to the ones used in a).
- c) The I/I_3^- electrolyte was prepared as per literature^[4]. Briefly, it was composed of 0.03M iodine, 0.6M 1-butyl-3-methylimidazolium Iodide, 0.5M tBp and 0.1 M guanidinium thiocyanate in DMF.
- d) The $[Co(bpy)_3]^{2+/3+}$ electrolyte was composed of 0.2M $[Co(bpy)_3](TFSI)_2$ and 0.06M $[Co(bpy)_3](TFSI)_3$ containing 0.1M 4-tert-butylpyridine (tBp) and 0.05M LiTFSI in N,N-dimethylformamide (DMF).

Device assembly:

DSCs were assembled using a 60 μ m thick surlyn gasket (inner dimensions 5 x 6 mm) in between the working and counter electrodes. The working electrode was pressed to the counter electrode using a pneumatic finger press while heating from the counter electrode side, effectively sealing the device. The electrolyte was vacuum backfilled into the cell cavity through a pre-drilled hole. The back of the pre-drilled hole was sealed using a surlyn coated aluminum sheet, which was prepared by laminating aluminum foil with a 25 μ m Surlyn sheet on a hot plate at 120°C.

Large Area Cells:

Silver paste preparation for working & counter electrode:

The silver paste was purchased from DuPont and used as received. Prior to the preparation of the working electrodes, the FTO glass substrates were cleaned, as indicated above for the small area cells, and then coated with a dense TiO_2 blocking layer by spray pyrolysis at 450°C by using a titanium diisopropoxide bis(acetylacetonate) (TAA) 7.5% in isopropanol solution. Counter electrodes were prepared without a blocking layer. The paste was screen printed on FTO glass using a commercial semi automatic screen printer, with a 90T mesh. One print was found to deposit 12 μ m thick silver layers. The films were sintered on a hot plate at 500°C for 30 minutes. The film thickness was measured using a Veeco Dektak 6m stylus profilometer. The dimension of the printed silver bus bar was 91x5 mm with silver grids (total: 15) being 81x1 mm with 5 mm gap in between grids (Total area of silver film: 16.7 cm^2).

Evaporated silver for external contact for working & counter electrode:

A silver film of around 100 nm thickness was thermally evaporated under high vacuum on top of the silver bus bar, extending across the Surlyn sealant, for creating an external contact while the rest of the substrate area was masked using a kapton sheet. The film thickness was measured using a Veeco Dektak 6m stylus profilometer.

TiO₂ working electrode preparation:

The TiO₂ paste was screen printed directly onto the FTO glass substrates equipped with the silver charge collectors (see above) using a commercial semi automatic screen printer, with a 90T mesh. One print was found to deposit 2 μm thick TiO₂ layers and a total of 3 layers were deposited. The printed transparent TiO₂ film thickness was measured to be 6 μm, using a Veeco Dektak 6m stylus profilometer. The dimensions of the printed films were 91 x 86 mm (Total area 78.26 cm², Active Titania Area: 60 cm²)

Zirconia spacer layer:

The zirconia paste was prepared following the method described by Thompson et al^[2]. A 4:1 ratio of 300 nm Ø and 20 nm Ø zirconia particles was used. The zirconia paste was printed on top of the silver surfaces and TiO₂ film using a 90T mesh. Each print was found to deposit a 2 μm thick ZrO₂ layer and the final printed ZrO₂ film thickness was measured to be 6 μm. The thickness of the films was measured using a Veeco Dektak 6m stylus profilometer. The dimensions of the printed films were 91 x 86 mm (Total area 78.26 cm²)

The films were sintered using a hot plate at 150°C for 10 minutes, at 325°C for 5 minutes, at 375°C for 5 minutes, at 450°C for 30 minutes and finally at 500°C for 15 minutes. After that, they were allowed to cool down and stored until further use.

Just before dye-sensitization, the working electrodes were reheated at 500°C for 30 minutes using a hot plate to remove absorbed water and organics from the TiO₂ surface. After cooling to 80°C, the films were immersed into the dye bath. Dye adsorption was achieved from a 0.3mM C106 dye solution (see Figure S1) in DMF containing 2mM chenodeoxycholic acid, used as a co-adsorbent. After 20 hours of dye coating, the films were rinsed in DMF and assembled to DSCs.

Carbon counter electrode preparation:

The carbon paste was screen printed on pre drilled FTO glass, equipped with a printed silver collection grid (see above) using a commercial semi automatic screen printer, with a 18T mesh. One print was found to deposit 10 to 12 μm thick carbon layers. The final printed carbon film thickness was measured to be 20 μm. The thickness of the films was measured using a Veeco Dektak 6m stylus profilometer. The dimensions of the printed films were 93x 88 mm (area 81.84 cm²)

Zirconia spacer layer

A zirconia spacer layer was printed on top of the counter electrode (silver grid and carbon layer) using the zirconia paste described above. The printed ZrO₂ film thickness was measured to be 6 μm, using a Veeco Dektak 6m stylus profilometer. The dimensions of the printed films were 91mm x 86 mm (Total area 78.26 cm²)

The counter electrode was sintered on a hot plate at 400°C for 30 minutes. After cooling, it was stored until use. Just before usage, it was reheated to 400°C for 30 minutes to remove absorbed water and organics from the carbon surface. After cooling to below 200°C, it was removed from the hot plate, rapidly cooled down on a thick metal plate (heat sink) and used immediately.

Device assembly:

DSCs were assembled by inserting a 60 µm thick surlyn gasket (inner dimensions 100 x 95 mm) in between the working and counter electrodes. A Kodak cell press was used to press the working electrode on to the counter electrode while heating the counter electrode. The back of the pre-drilled, filled hole was sealed using a U.V. epoxy (ThreeBond) after vacuum back filling of the electrolyte.

Device assembly for four wire sense experiments:

The plain glass substrates were coated with a dense TiO₂ blocking layer by spray pyrolysis at 450°C using a titanium diisopropoxide bis(acetylacetonate) (TAA) 7.5% in isopropanol solution. Silver was thermally evaporated to the surface under vacuum to a thickness of 100 nm at a rate of ~1nm/sec. The substrates were then laser etched to define a specific area, which would be exposed to the electrolytes. These substrates were then sealed with plain glass, equipped with a pre drilled hole, using a surlyn gasket. The electrolytes (a) 0.4M T_{ph} / 0.3M (T_{ph})₂ in DMF with 0.5M tBP and 0.05M LiTFSI and (b) 0.4M of T_{me} / 0.3M (T_{me})₂ in DMF with 0.5M tBP and 0.05M of LiTFSI were vacuum backfilled into the cell cavity. The back filling hole was sealed using an aluminum-Surlyn sheet on a hot plate at 120°C. The I⁻/I₃⁻ electrolyte c) composed of 0.03M iodine, 0.6M 1-butyl-3-methylimidazolium iodide, 0.5M tBP and 0.1 M guanidinium thiocyanate in DMF and the Co(bpy)₃^{2+/3+} electrolyte d) composed of 0.2 M of Co²⁺ and 0.06M of Co³⁺, 0.1M tBP, 0.05M LiTFSI in DMF were measured in an open cell set up due to the fast corrosion rates. In the case of open cell testing 20µl of electrolyte were drop casted onto the silver strip between the etch lines. A surlyn gasket (60 µm) had been melted on top of the device to define the exposed area. The exposed area for open and closed devices was 30 mm².

Electrochemical measurements:

- a) Four wire sense experiments were performed using a Keithley 2400 sourcemeter and in house made Labview software, to measure change in voltage periodically on applying constant current of 5 mA allowing to determine the change in resistance by applying Ohm's Law.
- b) Cyclic voltammetry experiments were performed using a VMP modular 5 channel potentiostat (BioLogic) with a three-electrode set up. The reference was a Ag/AgNO₃ that was calibrated against the Fc/Fc⁺ redox couple using a Pt disc working electrode and a Pt wire counter electrode by measuring the cyclic voltammogram of a 5mM ferrocene solution in acetonitrile containing 100 mM tetrabutylammonium hexafluorophosphate, TBAPF₆, as supporting electrolyte (E_{1/2} of Fc/Fc⁺ was taken as 630mV vs. NHE for the calibration). The redox reactions of the electrolytes on silver surfaces were characterized using printed Ag working electrodes (0.49 cm² silver film printed on FTO and sintered at

500°C for 30 min, 12 μm film thickness). The counter electrode was a glassy carbon disk electrode. The electrolytes a b and c were measured at a scan rate of 20mV/s. The working electrodes were soaked in the thiolate/disulfide based electrolytes solutions for 30 minutes prior to the experiment to reach a stable surface equilibrium, the $\text{Co}(\text{bpy})_3^{2+/3+}$ electrolyte was directly measured due to the rapid corrosion. The Rest Potentials of the $\text{Co}(\text{bpy})_3^{2+/3+}$ was measured to be -0.060 mV vs. Ag/AgNO_3 , for the $(\text{T}_{\text{me}})/(\text{T}_{\text{me}})_2$ electrolyte it was measured to be -0.317 mV and for the $(\text{T}_{\text{ph}})/(\text{T}_{\text{ph}})_2$ electrolyte -0.276 mV vs. Ag/AgNO_3 respectively. These electrolytes were scanned in the range of -700 to -900 mV, applied from their rest potentials for 5 cycles in order to determine their interaction with silver surface in the potential range of interest for solar cell operation.

Scanning tunneling microscopy measurements:

The substrate used for the SL-STM investigations was an atomically flat Ag (111) single crystal surface. The crystal was cleaned by consecutive Ar^+ -sputtering and annealing to 350°C in an ultra-high-vacuum chamber. It was afterwards put for one hour in a 0.4M T_{ph} or T_{me} solution in DMF. The sample was then washed in pure DMF solution and dried by Ar-gas blowing before putting it in the STM. The STM in use was an AGILENT 5100 STM, capable of scanning on a solid-liquid as well as on a solid-air interface. The surfaces were scanned either in air or in trichlorobenzene (TCB) solution for image enhancement^[6] at room temperature using constant current mode. STM images were processed using the WSXM software^[7].

Testing conditions for the subfigures of Figure 2 (main text) were a) $U_{\text{bias}} = 0.30 \text{ V}$, $I_t = 10.0 \text{ pA}$ b) $U_{\text{bias}} = 0.20 \text{ V}$, $I_t = 15.0 \text{ pA}$, c) $U_{\text{bias}} = 0.10 \text{ V}$, $I_t = 2.5 \text{ pA}$, d) $U_{\text{bias}} = 0.10 \text{ V}$, $I_t = 1.5 \text{ pA}$, e) $U_{\text{bias}} = 0.25 \text{ V}$, $I_t = 8.0 \text{ pA}$ and f) $U_{\text{bias}} = 0.25 \text{ V}$, $I_t = 9.0 \text{ pA}$

Device characterization:

An Oriel sun simulator (1,000 W Xe lamp) fitted with an AM 1.5 filter provided the light for the current voltage characterization of the small area DSCs. A silicon reference diode (Fraunhofer) equipped with a KG3 filter was used to calibrate the light intensity. Current density-voltage characteristics were measured utilizing a Keithley 2400 source meter and an in house made Labview software.

The large area DSCs were measured with a separate Oriel solar simulator optimized for the measurement of larger area devices, fitted with a 1000W Xe lamp, filtered to give an output of 100 mW cm^{-2} AM1.5 light intensity. The light intensity was calibrated using a Si reference solar cell from Peccell Limited, and was subsequently cross-calibrated with a reference Si cell traceable to the National Renewable Energy Laboratory. Current density-voltage characteristics were measured utilizing a Keithley 2400 Source meter and an in house made Labview software.

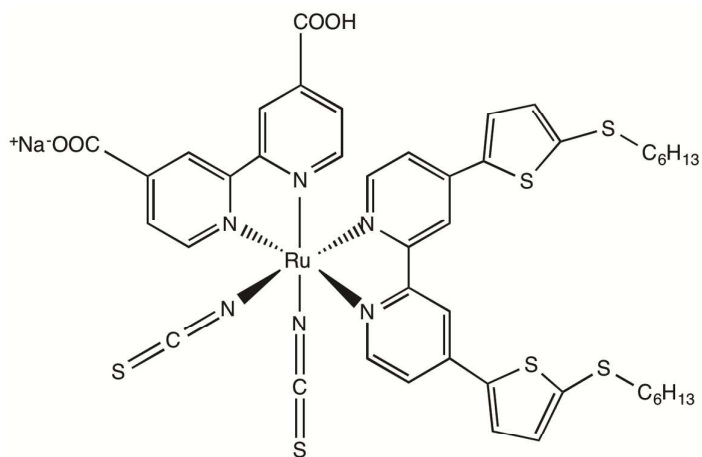
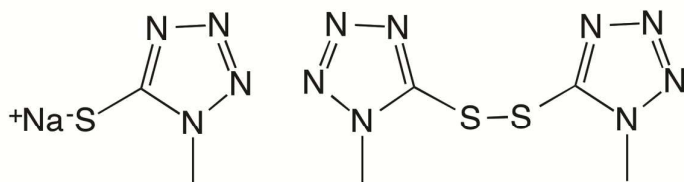


Figure S1: Ruthenium sensitizer C106 dye structure

(a)



(b)

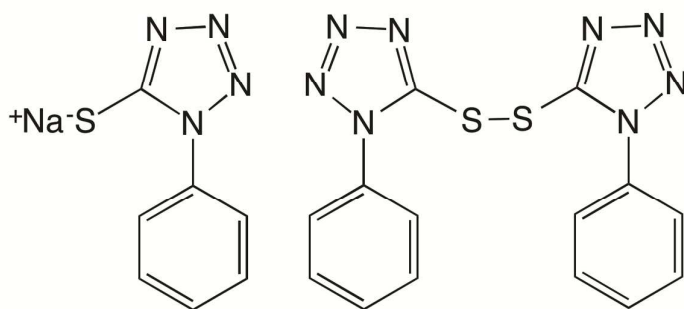


Figure S2: a) Structures of: a) sodium 5-mercapto-1-methyltetrazole (T_{me}) and di-5-(1-methyltetrazole)disulfide ($(T_{me})_2$); b) sodium 1-phenyl-1H-tetrazole-5-thiol (T_{ph}) and 5,5'-dithiobis(1-phenyl-1H-tetrazole) ($(T_{ph})_2$).

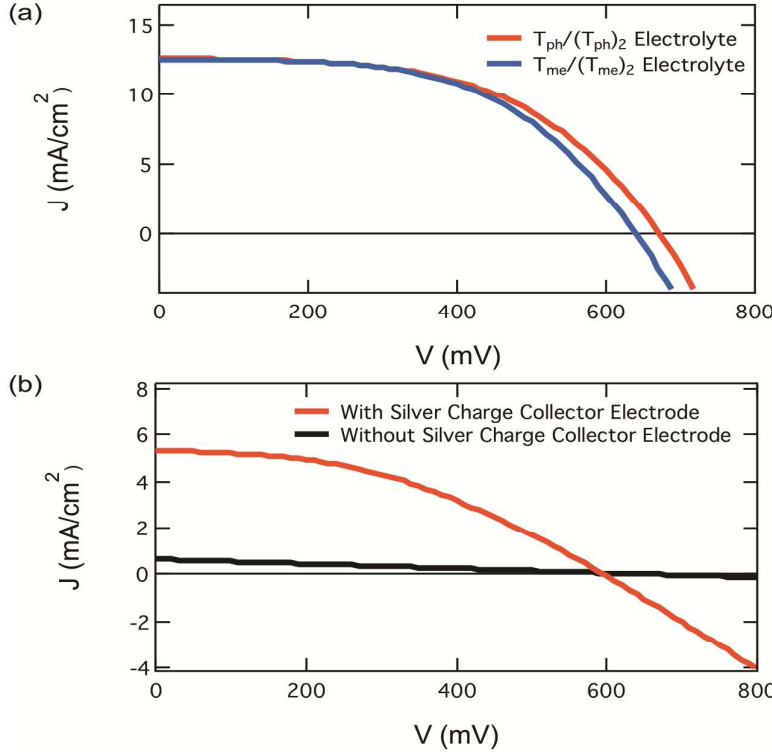


Figure S3: (a) IV curves of small area cells comparing $T_{ph}/(T_{ph})_2$ and $T_{me}/(T_{me})_2$ electrolytes (b) IV curve of the large area cells with and without silver charge collector electrode printed onto glass substrate

Table S1: Photovoltaic performance data for DSCs employing the two thiolate based redox couples and C106 dye, under simulated sunlight (AM 1.5 G, 1000 W/m²)

Redox couple ^[b]	Small Area Devices ^[a]		Large Area Devices ^[c]	
	$T_{me}/(T_{me})_2$	$T_{ph}/(T_{ph})_2$	Ag printed Electrodes	No Ag printed electrodes
V_{oc} (mV)	635±3	668±2	600	660
J_{sc} (mA cm ⁻²)	12.8±0.2	12.5±0.1	5.35	0.65
Fill Factor	0.53±0.01	0.52±0.01	0.41	0.24
η (%)	4.3±0.1	4.4±0.01	1.33	0.1

[a] Bi-layer TiO₂ films (6 μ m mesoporous TiO₂ (18 nm) and 6 μ m scattering TiO₂ (400 nm)) were used for the fabrication of small area DSCs with active area of 0.16 cm². A carbon counter electrode (20 μ m) was used. A minimum of three cells was tested. [b] The electrolyte consists of 0.40 M reduced species, 0.30 M of oxidised species, 0.05 M of LiTFSI and 0.50 M of tBp in DMF. [c] These columns represent the IV data of large area DSC device with and without silver charge collector electrode having an active area of 60 cm² and 78.6 cm² respectively.

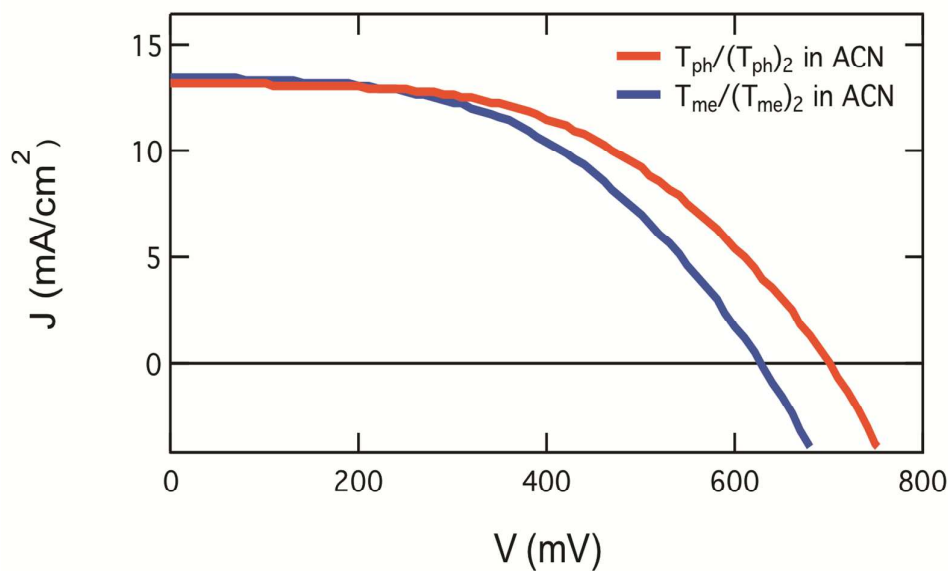


Figure S4: IV curve of small area DSCs made using $T_{ph}/(T_{ph})_2$ and $T_{me}/(T_{me})_2$ based electrolytes in acetonitrile. The electrolytes contain 0.40 M of the reduced species, 0.10 M of the oxidized species, 0.05 M of LiTFSI and 0.50 M of tBP.

Table S2: Tabulated photovoltaic data of the DSCs shown in Figure S3 utilizing acetonitrile based electrolytes and C106 dye tested under simulated sunlight (AM 1.5 G, 1000 W/m^2)^[a]

Redox couple ^[b]	$(T_{ph})/(T_{ph})_2$	$(T_{me})/(T_{me})_2$
Concentration of redox couple	0.4/0.1	0.4/0.1
V_{OC} (mV)	696 ± 3	630 ± 2
J_{SC} (mA cm^{-2})	12.9 ± 0.2	13.4 ± 0.6
FF	0.51 ± 0.01	0.48 ± 0.02
η (%)	4.6 ± 0.1	4.1 ± 0.1

[a] Double-layer TiO_2 films (6 μm mesoporous TiO_2 (18 nm) and 6 μm scattering TiO_2 (400 nm)) were used for the fabrication of all DSCs. A carbon counter electrode (20 μm) was used as counter electrode. The average performance with a standard deviation over 3 devices is provided. [b] The electrolytes consist of 0.40 M reduced species, 0.10 M of the oxidized species, 0.05 M LiTFSI and 0.50 M of tBP in acetonitrile.

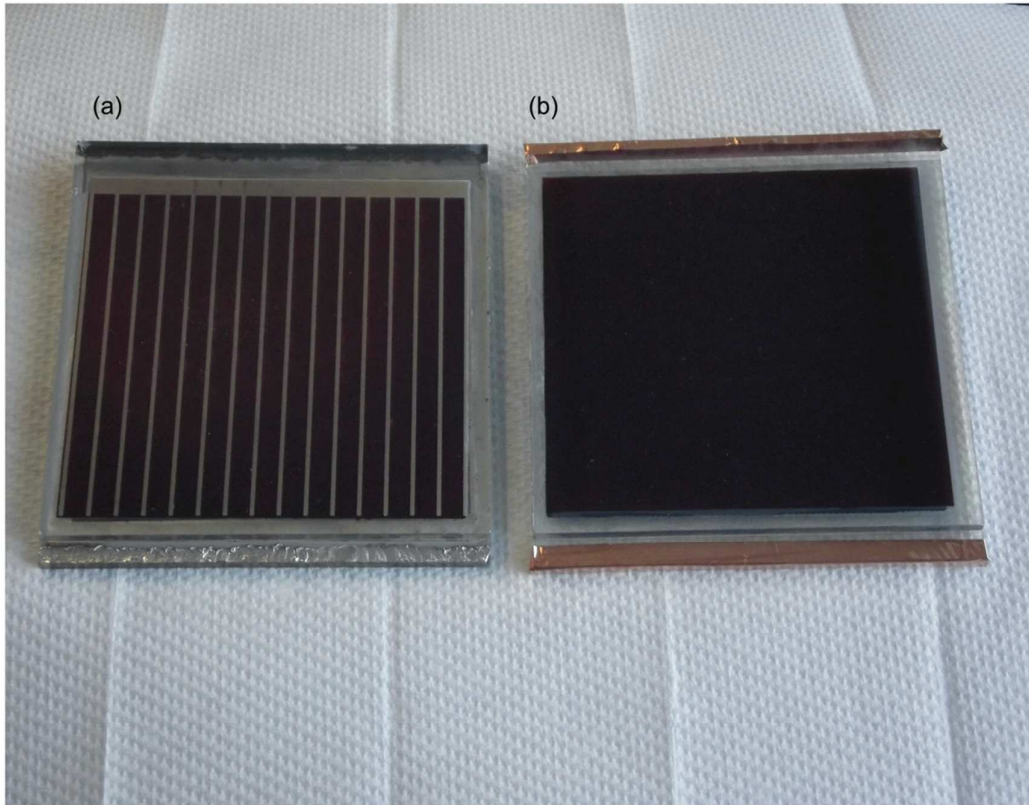


Figure S5: a) Large scale DSC printed with (a) and without (b) silver charge collector electrode.

References

- [1] Y. B. Yiming Cao, Qingjiang Yu, Yueming Cheng, Shi Liu, Dong Shi, Feifei Gao, and Peng Wang, *J. Phys. Chem. C* **2009**, *113*, 6290-6297.
- [2] S. J. Thompson, N. W. Duffy, U. Bach, Y.-B. Cheng, *J. Phys. Chem. C* **2010**, *114*, 2365-236
- [3] N. C. Mingkui Wang, Livain Breau, Jacques-E. Moser, Robin Humphry-Baker, Benôt Marsan, Shaik M. Zakeeruddin and Michael Grätzel, *Nat. Chem.* **2010**, *2*, 385-389.
- [4] aS. Powar, T. Daeneke, M. Ma, D. Fu, N. Duffy, G. Götz, M. Weidelener, A. Mishra, P. Bäuerle, L. Spiccia, *Angew. Chem. Int. Ed. Engl.* **2013**, *52*, 602, *Angew. Chem.* **2013**, *125*, 630-633.
- [5] W. Xiang, A. Gupta, M. K. Kashif, N. Duffy, A. Bilic, R. A. Evans, L. Spiccia, U. Bach, *ChemSusChem* **2013**, *6*, 256-260.
- [6] A. Ciesielski, C.-A. Palma, M. Bonini, P. Samori, *Adv. Mater.* **2010**, *22*, 3506-3520.
- [7] I. Horcas, R. Fernandez, J. Gomez-Rodriguez, J. Colchero, J. Gómez-Herrero, A. Baro, *Rev. Sci. Instrum.* **2007**, *78*, 013705.

CHAPTER 4
Future Work And Conclusion

Future work:

A major outcome of this work is the finding that the chemical structure of the 5-mercaptotetrazole is crucially important for its corrosion-protective properties. Corrosion rates varied by several orders of magnitude when comparing the methyl and phenyl derivative. While the corrosion rates for the phenyl-derivative was low, it was still too high to provide corrosion protection for Ag collector grids over the lifetime of a DSC module. In the future it would be interesting to further analyse the cause for these differences and how the molecular structure of the mercaptotetrazole affects its ability to form protective dense monolayers. This would involve a collaboration with theoreticians who can simulate the molecular self-assembly on silver surfaces for a wide range of different mercaptotetrazole derivatives with the aim to identify the next generation of corrosion-protective DSC electrolytes.

An alternative approach could involve the replacement of the metal used in this study to form the collector grid (silver) to less corrosive materials such as chromium or nickel.

In the research presented in this thesis, a significant effort was made to optimize solar cells as a plethora of counter electrode materials were investigated before carbon was selected as being the choice of counter electrode. Designing a module device and its stability are still an issue which needs to be addressed since the current proof of principle device architecture is still flawed due to the use of evaporated silver needed to create external contacts on both working and counter electrodes of the large area DSCs. The evaporated silver is oxidized while sintering the electrodes, leading to increased series resistance in the device. The sealing with surlyn is still not the optimal choice of sealant as it frequently leads to faulty sealing and the leakage of electrolyte. With carbon acting as counter electrode, back filling of electrolyte can be an impediment as it acts as a visual block.

Thus, the next round of research and focus need to be given on the following thrust areas, so that better designed and higher efficiency solar cells can be created and if possible commercialized as well:

4.1 Characterization of alternate metals as corrosion resistant metals and alternate 5 mercaptotetrazole derivatives as corrosion inhibitors

- Alternate metals, gold, copper, tungsten, stainless steel and nickel can be investigated.
- Nickel has been used for charge collectors in large scale DSCs previously in combination with an iodine based electrolyte. After initially promising results this metal / electrolyte combination is currently not seen as a viable option due to slowly progressing corrosion^[1].
- Copper metal corroded within a matter of minutes on exposure to the electrolyte, as it tends to form Cu^+ complexes with the thiolates.
- Tungsten metal needs investigation

4.2 Thiolate/disulfide based electrolytes for p-type and tandem dye-sensitized solar cells

- Investigate tandem dye-sensitized solar cell dyes which can be fabricated with complementary absorption spectra in conjunction with optically transparent, non corrosive and organic thiolate/disulfide based electrolyte.
- Investigate other forms of thiolate based electrolytes with ptype DSCs to achieve higher efficiencies.

4.3 Alternate metals as corrosion resistant metals and alternate 5 mercaptotetrazole derivatives as corrosion inhibitors

- Investigate alternate metals which can be more corrosion resistant metals compared to silver and alternate thiolates which can act as better corrosion inhibitors
- Characterize the corrosion inhibition and blocking contact properties utilizing four-wire sense measurement and cyclic voltammetry.

- Characterize with standard corrosion testing methods to quantify the rate of corrosion.
- Develop a theoretical model to understand surface passivation and corrosion inhibition properties of different thiolates and corrosion resistant properties of different metals based on the structure of the thiolates and their orientation onto metals.

4.4 Alternate metals as charge collectors and alternate 5-mercaptotetrazole derivatives as redox mediators

- From the previous study, pick out the best alternate metal which can be utilized as charge collectors in DSCs as a replacement to silver charge collectors in DSCs
- From the previous study, pick out the best alternate 5-mercaptotetrazole derivatives which can be utilized as a redox mediator
- Optimize small and large area solar cells and characterize their photo electrochemical performance using IV and IPCE techniques
- Characterize the different 5-mercaptotetrazole derivatives using Transient absorption spectroscopy to understand their dye regeneration kinetics.
- Characterize the electron lifetime of the different 5-mercaptotetrazole derivatives using IMVS and IMPS techniques

4.5 Fully Printed large area Monolithic DSCs

- Up scaling DSCs has always been a challenge and TCO has been a major cost contributor in DSCs. Designing TCO free modules has been hindered due to corrosive electrolytes employed in DSCs
- Having investigated non-corrosive electrolytes, it gives us an advantage of being able to develop novel architectures for DSCs.
- Without the need of protecting the metal charge collectors we have the advantage and flexibility to be able to design monolithic module architectures

which can have higher active areas due to the increased fill ratio of the module

$$\left(\frac{A_{\text{TiO}_2} - A_{\text{charge collector}}}{A_{\text{TiO}_2}}\right)$$

- Characterize the different printed layers using SEM
- Characterize the current flow through the module utilizing photocurrent-mapping.
- Characterize the photo electrochemical performance using IV and IPCE measurements.

Conclusion:

More than two decades have passed since dye sensitized solar cells were introduced, and over the past few years we have seen a shift in research focus from iodine-based systems to alternate redox electrolytes. The main driving force besides efficiency enhancement has been the scope find alternative electrolytes, which are non corrosive and more benign. The corrosive nature of iodine based electrolytes is also a deterrent in designing new architectures for DSCs and the application of charge collector grids.

In this thesis, a new class of thiolate based electrolytes was investigated for their non corrosive nature towards silver charge collector lines and in addition to their application in p-type dscs.

The new class of electrolytes, 5-mercaptotetrazoles have surface passivating properties, which were found to be highly dependent on their chemical structure. A comparison study of two 5-mercaptotetrazole derivatives was carried out, which revealed that a simple substitution of a methyl group with a phenyl group fundamentally changes the self-assembly properties and accordingly leads to an improved ability to form a protective monolayer on metal electrodes. Thus, we showed that 5-mercaptotetrazoles can be used as a dual function agent in DSCs: firstly, as a surface passivating agent, impeding corrosion and recombination across the metal-electrolyte interface and, secondly, as the redox mediators, accomplishing quantitative dye-regeneration.

We observed that iodine and cobalt based standard electrolytes exhibited electrochemical potentials, which were thermodynamically suitable not only to ensure

quantitative dye regeneration but also lead to corrosion of metals such as silver. The latter is a significant impediment towards the application of metals as charge collection electrodes.

Due to their electrochemical potential, 5-mercaptotetrazoles are capable of oxidizing silver electrodes, yet in this study we show that their strong interaction with silver surfaces results in the formation of a self-assembled monolayer impeding their own redox reactions. This has two desirable consequences: firstly the surface passivation results in a strong suppression of silver corrosion and, secondly, a high over potential for the reduction of the corresponding disulfides of 5-mercaptotetrazole at the silver electrode of the photoanode. The latter results in the suppression of the recombination reaction between the separated charges via the Ag metal surface.

Both, the suppression of the corrosion process and the interfacial recombination losses are necessities for the application of the redox electrolyte in direct contact with the charge collecting electrode. This allowed us to fabricate a fully printable prototype device with an improved fill ratio since no protective layers had to be deposited on top of the charge collection grids.

While the corrosion rates observed for T_{ph} were exceptionally low, the actual corrosion process itself over the period of several years could still be problematic for the application of unprotected silver electrodes in DSCs. Nevertheless, the strong correlation revealed here between the molecular structure of the two 5-mercaptotetrazoles and their surface passivation properties provides a strong stimulus for the design and development of the next generation of thiolate-based redox mediators with further improved self-assembly and corrosion-protection properties.

In addition, 5-methyl mercaptotetrazoles based electrolyte (T_{ph}) was also investigated in p-type and pn-DSCs. We observed that applying these thiolate based electrolytes resulted in an improvement in V_{OC} in p-DSCs compared to the devices based on iodide electrolytes, while maintaining similar J_{SC} (5.3 mA/cm^2) values. We also employed the T_{ph} electrolyte in tandem DSCs with film thicknesses optimized for both the T_{ph} and iodine based electrolytes, we observed that the tandem cells based on the non-corrosive thiolate electrolyte exhibited similar conversion efficiencies

(1.33 %) to those based on iodide electrolytes (1.28 %). Our results reveal the great promise which the thiolate based electrolytes holds for future applications in p-DSCs and pn-DSCs.

In conclusion, further studies are needed to fully reveal the maximum potential of thiolate-based electrolytes. The key advantages of thiolate based electrolytes lies in the fact that they have optical transparency in the visible region, favorable rest potential and non-corrosive properties, which place them ahead of iodide and cobalt based redox couples for a number of applications such as large scale DSC modules, novel architectures and designs of DSC modules, p-DSCs and pn-DSCs.

CHAPTER 5

Thiolate/Disulfide Based Electrolytes for p-type and Tandem Dye-Sensitized Solar Cells

Monash University

Declaration for Thesis Chapter [5]

Declaration by candidate

In the case of Chapter [5], the nature and extent of my contribution to the work was the following:

Nature of contribution	Extent of contribution (%)
All experimental work, preparation of manuscript and editing	10

The following co-authors contributed to the work. If co-authors are students at Monash University, the extent of their contribution in percentage terms must be stated:

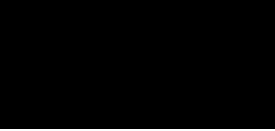
Name	Nature of contribution	Extent of contribution (%) for student co-authors only
Torben Daeneke	Dye synthesis, drafting and editing	N/A
Satvasheel Powar	Experimental design and planning, drafting and editing	60
Günther Götz	Data analysis, drafting and editing.	N/A
Peter Bäuerle	Drafting and editing	N/A
Frank A. Nüesch	Drafting and editing	N/A
Leonne Spiccia	Drafting and editing	N/A
Udo Bach	Experimental design and planning, drafting and editing	N/A

The undersigned hereby certify that the above declaration correctly reflects the nature and extent of the candidate's and co-authors' contributions to this work*.

Candidate's Signature

	Date 13.01.16
---	---------------

**Main
Supervisor's
Signature**

		Date 13.01.16
---	--	----------------------



Thiolate/Disulfide Based Electrolytes for p-type and Tandem Dye-Sensitized Solar Cells



Satvasheel Powar^{a,b,*}, Rishabh Bhargava^c, Torben Daeneke^{d,e}, Günther Götz^f, Peter Bäuerle^f, Thomas Geiger^g, Simon Kuster^h, Frank A. Nüesch^g, Leone Spiccia^a, Udo Bach^{c,d,i,*}

^a School of Chemistry, Monash University, Clayton, Victoria, 3800, Australia

^b School of Engineering, Indian Institute of Technology Mandi, Mandi, Himachal Pradesh, 175001, India

^c Department of Materials Engineering, Monash University, Clayton Victoria, 3800, Australia

^d Commonwealth Scientific and Industrial Research Organization, Materials Science and Engineering, Clayton South, Victoria 3169, Australia

^e School of Electrical and Computer Engineering, RMIT University, 3000 Melbourne, Victoria, Australia

^f Institute of Organic Chemistry II and Advanced Materials, University of Ulm, Albert-Einstein-Allee 11, 89081 Ulm, Germany

^g Laboratory for Functional Polymers, Swiss Federal Laboratories for Materials Science and Technology (Empa), Überlandstrasse 129, 8600 Dübendorf, Switzerland

^h Institute of Food, Nutrition and Health (IFNH), ETH Zurich, Schmelzbergstrasse 9, 8092 Zürich, Switzerland

ⁱ Melbourne Centre for Nanofabrication, 151 Wellington Road, Clayton, VIC 3168, Australia

ARTICLE INFO

Article history:

Received 2 July 2015

Received in revised form 28 August 2015

Accepted 5 September 2015

Available online 8 September 2015

Keywords:

Thiolate/Disulfide Electrolyte
p-type dye-sensitized solar cells
tandem dye-sensitized solar cells
redox electrolyte
p-DSC

ABSTRACT

This article presents the first report of a tandem dye-sensitized solar cell employing optically transparent, non-corrosive metal-free thiolate/disulfide based electrolytes and a set of sensitizers with complementary absorption spectra. Sodium 1-phenyl-1H-tetrazole-5-thiolate and its reduced form 5,5'-dithiobis(1-phenyl-1H-tetrazole) (thiolate/disulfide) were used as redox mediators for photocathodic dye-sensitized solar cells (p-DSCs), yielding higher open circuit voltages (285 mV) compared to the more commonly used iodide-based redox couple (226 mV). The herein achieved efficiencies of p-DSCs (0.51 %) and pn-DSCs (1.33 %) employing the thiolate/disulfide-based electrolytes were comparable to p-DSCs and pn-DSCs employing conventional iodide-based electrolytes (0.44 % and 1.19 %).

© 2015 Elsevier Ltd. All rights reserved.

Dye-sensitized solar cells (DSCs) with their low projected costs have increasingly attracted attention as an alternative to silicon solar cells [1,2]. The highest reported conversion efficiencies for dye-sensitized photoanodes (n-DSCs) and dye-sensitized photocathodes (p-DSCs) are 13% and 2.5% respectively, under simulated sunlight (1000 W/m², AM1.5 G) [3,4]. These record efficiencies still lag behind the conventional silicon solar cells and some other thin film solar cell technologies. Researchers have been endeavouring to improve the efficiencies of n-DSC and p-DSC by altering the semiconductors, sensitizers and redox couples [3–24]. One attractive approach to improve efficiencies is to construct third generation tandem dye-sensitized solar cells (pn-DSCs). In the n-DSCs, the photocurrent results from dye-sensitized electron injection into n-type semiconductors, e.g. TiO₂, whereas in p-

DSC electron transfer occurs from the valence band of the p-type semiconductor (NiO being the most commonly used to date) to the photoexcited dye [25,26]. These charge separation mechanisms are complementary and provide the opportunity to assemble n-DSCs and p-DSCs in a simple sandwich structure to produce tandem dye-sensitized solar cells (pn-DSCs) [27]. According to Kirchoff's circuit law photovoltages are additive for this type of pn-DSCs, as the photoelectrodes are connected in series. However, the photocurrent is limited by the weaker performing photoelectrode [27,28].

Previously reported pn-DSC efficiencies have been higher than their individual components (n-DSCs and p-DSCs). However, those devices still shared several limitations. The overlapping absorption spectra of the most efficient p-DSC sensitizer (PMI-6T-TPA – see Fig. 1a) with that of the applied n-DSC sensitizers (N719) meant that both photoelectrodes were competing for photons in a similar wavelength range, limiting the attainable pn-DSC photocurrent. Furthermore, the tandem devices were utilizing electrolytes based on the I⁻/I₃⁻ redox couple which absorbs strongly at wavelengths below 500 nm [6].

* Corresponding authors.

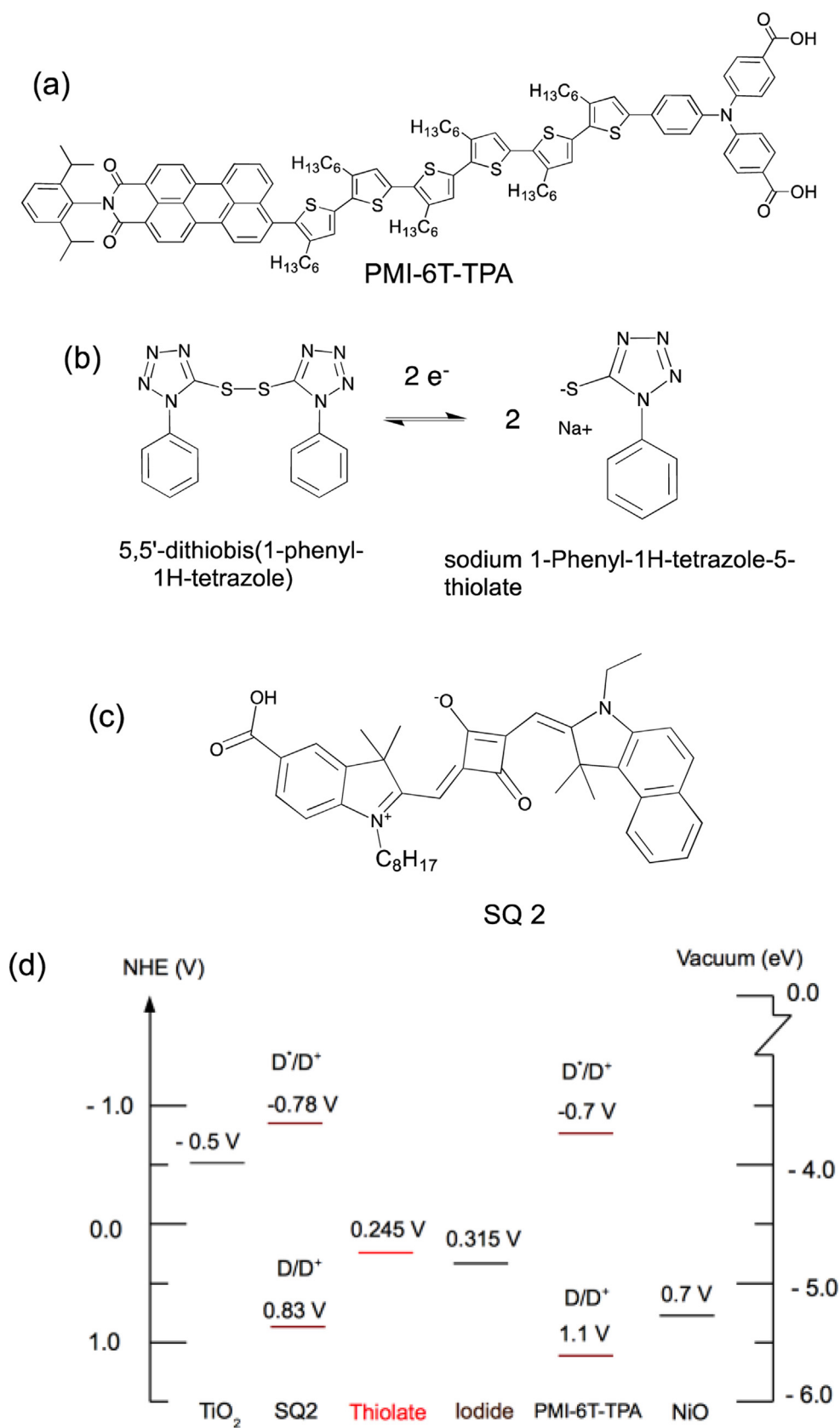


Fig. 1. (a) Structure of the PMI-6T-TPA sensitizer [29]; (b) structures of the oxidized (5,5'-dithiobis(1-phenyl-1H-tetrazole)) and reduced (sodium 1-phenyl-1H-tetrazole-5-thiolate) forms of the redox couple; (c) structure of the SQ2 sensitizer; (d) approximate energy diagram for the components used in the tandem solar cells with the rest potentials of the iodide and thiolate electrolytes (measured according to a literature procedure) [30]. The work functions of NiO (- 5.2 eV) and the sensitizer were measured using photoelectron spectroscopy (PESA) (Figure S1, ESI †) and the conduction band edge of TiO₂ (- 4.0 eV) was taken from the literature [11,29,31].

Table 1
Photovoltaic performance parameters for p-DSCs, n-DSCs and pn-DSCs under one sun simulated sunlight (1000 W/m², AM1.5G). The tandem pn-DSCs and n-DSCs were illuminated through the n-side (TiO₂) and the p-DSCs were illuminated through the p-side (NiO).

	Thiolate electrolyte ^[a]		
	p-DSC	n-DSC	pn-DSC
V _{OC} (mV)	285 ± 10	595 ± 6	814 ± 18
J _{SC} (mA/cm ²)	5.3 ± 0.5	2.6 ± 0.3	2.5 ± 0.2
Fill Factor	0.34 ± 0.01	0.64 ± 0.04	0.65 ± 0.05
Efficiency (%)	0.51 ± 0.03	1.00 ± 0.05	1.33 ± 0.02
	Iodide electrolyte ^[b]		
	p-DSC	n-DSC	pn-DSC
V _{OC} (mV)	226 ± 4	718 ± 8	924 ± 13
J _{SC} (mA/cm ²)	5.3 ± 0.3	3.6 ± 0.1	1.9 ± 0.1
Fill Factor	0.36 ± 0.01	0.77 ± 0.01	0.67 ± 0.02
Efficiency (%)	0.44 ± 0.02	1.97 ± 0.05	1.19 ± 0.04

^a [a],[b] See Experimental Section for electrolyte compositions. The p-DSCs were based on mesoporous NiO electrodes (film thickness = 1.8 μm and surface area = 0.16 cm²) sensitized with PMI-6T-TPA, n-DSC were based on mesoporous TiO₂ electrodes (film thickness = 2 μm and surface area = 0.16 cm²) sensitized with SQ2 dye.

Iodide/triiodide had been the most commonly applied redox couple for both n-DSCs and p-DSCs. Concerns over the corrosive nature and complex redox chemistry of this redox couple has led researchers to explore alternative redox mediators [32]. In recent years major advances have been made resulting in the application of metal complexes (Co, Fe and Ni) and organic thiolate based redox mediators [10,33–38]. Interest in thiolate/disulfide as alternative redox couple in n-DSCs has been growing very rapidly, due to its non-corrosive properties and optical transparency [10,33–37].

Overall, the realization of high efficiency pn-DSCs requires: (i) the development of p-DSC and n-DSC sensitizers with complementary absorption spectra; (ii) new p-type semiconductors with higher ionization potential and/or alternative n-type semiconductors with lower conduction band edge to improve the open circuit voltage (V_{OC}); and (iii) optically transparent electrolytes. This report is attempting to address requirements (i) and (iii).

Here, we report the application of an optically transparent thiolate/disulfide electrolyte based on (5,5'-dithiobis(1-phenyl-1H-tetrazole)) and sodium 1-phenyl-1H-tetrazole-5-thiolate as redox couple (see Fig. 1(b)) in p-DSCs and tandem pn-DSCs. The redox potential of the thiolate electrolyte (245 mV vs. NHE) is about 70 mV more negative than that of the iodide electrolyte (315 mV vs. NHE), offering an opportunity to improve the V_{OC} of p-DSCs. The theoretical open circuit voltage of p-DSC is defined by the difference of the quasi-Fermi-level in the p-type semiconductor and the redox potential of the electrolyte.

The photovoltaic performances of p-DSCs employing these two electrolytes were measured under simulated sunlight (1000 W/m², AM 1.5G) and are summarized in Table 1 (current-voltage characteristics are shown in Figure S2, ESI †). The V_{OC} of iodide-based p-DSCs (226 mV) together with the short-circuit current (J_{SC}) of 5.3 mA/cm² yielded an overall efficiency of 0.44%, comparable to literature reports [16,28]. Replacing the iodide electrolyte with a thiolate electrolyte improved the V_{OC} by ~60 mV (285 mV). This V_{OC} improvement is very close to the expected V_{OC} shift due to difference in the electrolyte rest potentials (c 70 mV). The improved V_{OC} and identical J_{SC} values (5.3 mA/cm²) lead to an increase in the overall efficiency of thiolate/disulfide based p-DSCs to 0.51%, compared to iodide based p-DSCs (0.44%).

In order to realize high pn-DSC efficiency, either of the two electrodes is required to absorb and efficiently convert photons from the red and near infrared section of the solar spectrum. Near infrared (near IR) dyes can be applied to either the p-DSC or n-DSC. However, infrared sensitizers reported in the literature are limited to n-DSCs [29,39–41]. The squaraine-based sensitizer SQ2 (Fig. 1c) developed by the groups of Nüesch and Grätzel features a strong

absorption peak at 675 nm and a window of low absorption in the range from 400 nm to 580 nm [29]. It is spectrally complementary to the best performing p-type sensitizer PMI-6T-TPA. Fig. 2 shows IPCE spectra of p-DSC and n-DSC employing the thiolate based electrolyte. The p-DSC and n-DSC sensitizers show complementary absorption spectrum.

Since the overall J_{SC} value of a series connected tandem solar cell is limited by the electrode producing the lower J_{SC}, both photoelectrodes have to be carefully optimized and matched, to maximize the efficiency of pn-DSCs. The light harvesting properties of each electrode can be adjusted by controlling the film thickness of the NiO and TiO₂ films.

The maximum theoretical photocurrent of a single junction dye-sensitized solar cell can be calculated based on its light harvesting efficiency and absorbed photon to charge carrier conversion efficiencies (APCE) (equation 1) [16]. Based on the single junction solar cell calculation model, we have extended the J_{SC} calculation model to assist in tandem solar cell electrode thickness optimization. In the pn-DSC calculations, the light reaching the second photoelectrode was estimated by taking into account the transmission losses that occur in the top electrode and electrolyte layer. The expected J_{SC} values of pn-DSCs for a range of photoelectrode film thicknesses were calculated based on the absorption properties of the individual cell components and the APCEs for both photoelectrodes. A detailed derivation can be found in the ESI †.

$$J_{SC} = \frac{e}{hc} \int \phi_p AM1.5G(\lambda) \cdot LHE(\lambda) \cdot \phi_{inj} \cdot \phi_{cc} \cdot d\lambda \quad (1)$$

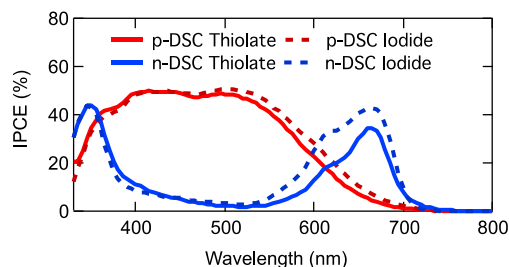


Fig. 2. IPCE spectra of a p-DSC (red line) and n-DSC (blue line) comprising a thiolate electrolyte. For comparison the IPCE spectra of a p-DSC (dotted red line) and n-DSC (dotted blue line) in conjunction with an iodide-based electrolyte are also shown. p-DSCs were constructed from PMI-6T-TPA sensitized mesoporous NiO electrodes (thickness: 1.8 μm). n-DSCs were constructed from SQ2 sensitized mesoporous TiO₂ electrodes (thickness: 2 μm). For the electrolyte composition see Experimental Section. (For interpretation of the references to color in this figure legend, the reader is referred to the web version of this article.)

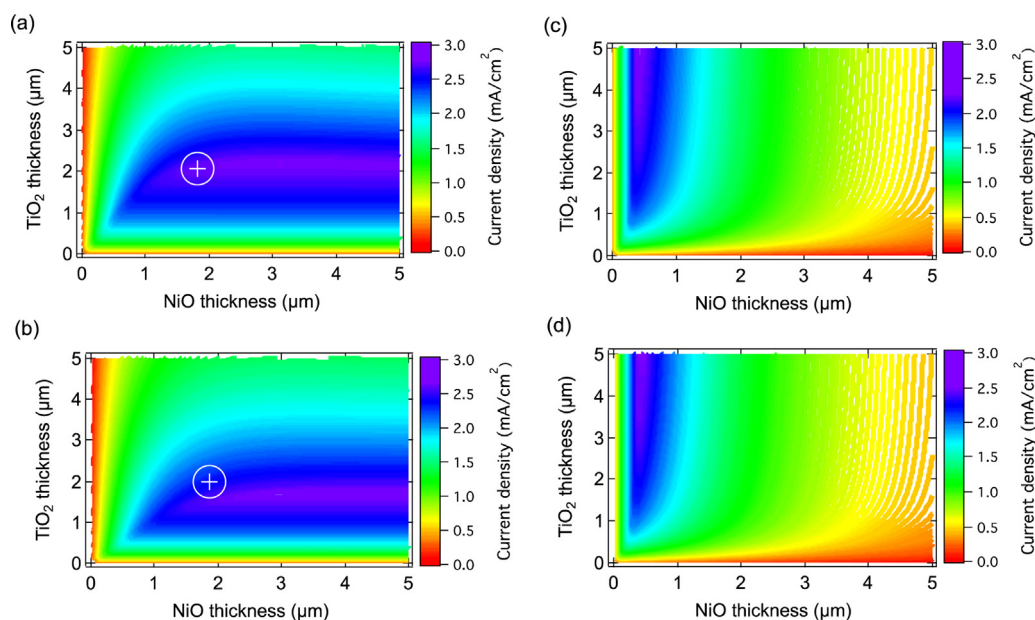


Fig. 3. Calculated photocurrent density (J_{sc}) estimate at one sun irradiation (1000 W/m^2 , AM 1.5 G) of tandem pn-DSCs [illuminated through the TiO_2 electrode side (a), (b) and the NiO electrode side (c), (d)] using a thiolate electrolyte (a), (c); and an iodide electrolyte (b), (d). The crosshair shows the respective film thicknesses used to prepare the DSCs reported in Table 1.

The absorptivity of both electrolytes was measured using a $22.5 \mu\text{m}$ path length cuvette; corresponding to the electrolyte layer thickness in DSCs (Fig. S3). In accordance with previous reports [10,33–37], the thiolate electrolyte showed negligible absorption in the visible spectral range, while the iodide electrolyte significantly absorbs light at wavelengths below 490 nm . The results highlight the advantage of the new thiolate based electrolyte for pn-DSCs in which the incident light has to pass through the electrolyte compartment to reach the bottom electrode. APCE values for p-DSCs and n-DSCs employing thiolate and iodide electrolytes were determined experimentally (see Table S1) and assumed to be independent of the layer thickness. The APCEs for p-DSCs sensitized with PMI-6T-TPA, employing thiolate and iodide electrolytes were determined to be 0.92 and 0.95, respectively. The measured APCE values for SQ2 sensitized n-DSCs employing thiolate and iodide electrolyte were 0.38 and 0.40 respectively, much lower compared to p-DSCs.

Fig. 3 shows a contour graph of the calculated tandem solar cell J_{sc} values, illuminated through TiO_2 , as a function of TiO_2 and NiO film thicknesses for both electrolytes. The calculation predicts maximum photocurrents of about 2.82 mA/cm^2 and 2.24 mA/cm^2 in tandem pn-DSCs for optimized TiO_2 thicknesses of $2 \mu\text{m}$ and $1.6 \mu\text{m}$ in conjunction with thiolate and iodide electrolytes respectively. This indicates that the absorption of the iodide electrolyte imposes additional restrictions to the top electrode thickness. The stronger inner filter effect in iodide-based tandem cells needs to be compensated by employing a thinner TiO_2 top electrode, to ensure sufficient light penetration to the underlying NiO electrode.

The tandem solar cell J_{sc} contour graphs for pn-DSCs using thiolate electrolyte and iodide electrolyte with an illumination through the NiO electrode are shown in Fig. 3c and d respectively. A similar maximum J_{sc} of $\sim 2.54 \text{ mA/cm}^2$ can be expected in this illumination mode with comparably thin NiO top electrodes ($0.5 \mu\text{m}$). Here the self-absorption of the NiO semiconductor film introduces an additional inner filter effect.

Table 1 summarizes the J-V performance data of p-DSCs, n-DSCs and the tandem pn-DSCs, measured under simulated sunlight

(1000 W/m^2 , AM 1.5 G). The corresponding J-V curves are shown in Fig. S2 (ESI †). The pn-DSCs using the thiolate electrolytes were found to be slightly more efficient (1.33 %) than those comprising an iodide electrolyte (1.19 %), even though the efficiency of n-DSC using the thiolate electrolyte (1.00 %) was lower than for the iodide-based n-DSC (1.97 %).

The NiO and TiO_2 film thicknesses used for these devices were optimized for pn-DSCs employing a thiolate-based electrolyte. According to the results of our simple photocurrent calculation in Fig. 3 the semiconductor film thickness used for the devices reported in Table 1 are not ideal for iodide based pn-DSCs. Assembling pn-DSCs with film thicknesses optimized for iodide-based cells according to Fig. 3b indeed yielded an improved photocurrent (2.6 mA/cm^2) and device efficiency (1.28 %; see Table S2, ESI †), comparable to the optimized thiolate-electrolyte based pn-DSC.

Generally, the photocurrent trends observed in pn-DSCs follow the calculations depicted in Fig. 3, while the magnitude of the measured photocurrents at full sun illumination generally turned out lower than predicted. This effect can be attributed to the sub-linear dependence of photocurrent and illumination intensity, generally observed for the DSCs presented here. Table S3 shows the performance data of the devices described in Table 1 at 1/10 sun simulated sunlight (100 W/m^2 , AM1.5 G). Here the photocurrents of 0.27 and 0.30 mA/cm^2 for iodide and thiolate electrolyte based pn-DSCs respectively are generally in good agreement with the calculated values illustrated in Fig. 3.

The V_{oc} for iodide based pn-DSCs characterized in Table 1 is about 110 mV higher than for thiolate-based tandem DSCs. The nature of the redox mediator should, however, not directly affect the V_{oc} , which should correspond to the difference of the quasi-Fermi levels in the NiO and TiO_2 electrode under illumination. An interpretation of the difference in V_{oc} between these tandem solar cells is difficult, as the optimized thiolate and iodide electrolytes employed here varied strongly in their composition (see Experimental Section). Above all, the absence of flatband determining lithium ions in the iodine electrolyte and the presence of 50 mM Li^+ in the thiolate electrolyte is expected to strongly affect the V_{oc} of n-DSCs. Indeed we observe that the

addition of 50 mM Li⁺ to iodide electrolyte drastically drops the V_{OC} of the iodide-based pn-DSC (750 mV) below that of the thiolate pn-DSC (see Table S3 ESI †).

1. Experimental

Two electrolytes were prepared; (a) an optimized thiolate electrolyte [0.05 M 5,5'-dithiobis(1-phenyl-1H-tetrazole), 0.40 M sodium 1-phenyl-1H-tetrazole-5-thiolate, 0.05 M lithium bis(trifluoromethanesulfonylimide), 0.50 M 4-tert-butylpyridine in acetonitrile]; and (b) an optimized iodide electrolyte [0.03 M iodine, 0.6 M 1-butyl-3-methylimidazolium iodide, 0.5 M 4-tert-butylpyridine and 0.1 M guanidinium thiocyanate in 85:15 acetonitrile: valeronitrile]. p-DSC were constructed following the literature procedures (see ESI † for details) [42]. Briefly, for p-DSCs sintered 1.8 μm thick mesoporous nickel(II) oxide (NiO) electrodes were sensitized in a 0.2 mM PMI-6T-TPA dye solution (in DMF) for 2 hours and rinsed before they were used to construct p-DSCs with counter electrodes. The electrolytes were vacuum back filled through a predrilled hole on the counter electrode. Platinized conducting glass counter electrodes were used for the iodide electrolyte based devices. However, since the thiolate based electrolytes have a very high charge transfer resistance on platinum, poly(3,4-ethylenedioxythiophene) (PEDOT) counter electrodes were used in thiolate based p-DSCs (Figure S6, ESI †) [37]. For n-DSCs 2 μm thick TiO₂ electrodes were sensitized in 0.2 mM SQ2 dye solution (in ethanol), with the addition of 10 mM chenodeoxycholic acid. For tandem solar cells TiO₂ electrodes were drilled for electrolyte back filling, prior to dyeing. The tandem solar cells were assembled using dyed TiO₂ electrodes and NiO electrodes. More details on experimental procedures are in ESI †.

2. Conclusions

We have demonstrated a tandem dye-sensitized solar cell with complementary absorption of the photocathodic and photoanodic sensitizers that utilize an optically transparent, non-corrosive organic thiolate based electrolyte. We have developed a simple model for optimizing the film thicknesses of photoelectrodes for tandem DSC applications. The developed thiolate based electrolyte resulted in an improvement in V_{OC} in p-DSCs compared to the devices based on iodide electrolytes, while maintaining similar J_{SC} (5.3 mA/cm²) values. When employed in tandem DSCs with film thicknesses optimized for the two respective electrolytes the tandem cells based on the non-corrosive thiolate electrolyte exhibited similar conversion efficiencies (1.33 %) to those based on iodide electrolytes (1.28 %). Our results reveal the great potential of thiolate based electrolytes for future applications in p-DSCs and pn-DSCs. The optical transparency in the visible region, favorable rest potential and the noncorrosive nature of the thiolate redox couple makes it more suitable than the iodide based redox couple for these applications. Future studies should focus on developing novel near IR dyes with the potential to generate higher photocurrents, which can boost the efficiencies even further. Novel semiconductors with improved conduction and valence band positions should be developed in order to increase the open circuit potential of pn-DSCs. The difference between the n-type semiconductors conduction band and the p-type semiconductors valence band should be significantly increased. Future research should focus on identifying suitable semiconductor/dye combinations for both n- and p-type devices that fulfil this requirement. Furthermore research identifying the suitable requirements for high efficiency pn-DSCs should be conducted.

ACKNOWLEDGMENT

The authors acknowledge the Australian Research Council for providing equipment and fellowship support and the Australian Solar Institute, the Victorian State Government (DBI-VSA and DPI-ETIS) for financial support. The Commonwealth Scientific and Industrial Research Organization is acknowledged for providing support through an OCE Science Leader position (UB). This work was performed partly at the Melbourne Centre for Nanofabrication, an initiative partly funded by the Commonwealth of Australia and the Victorian Government.

Appendix A. Supplementary data

Supplementary data associated with this article can be found, in the online version, at <http://dx.doi.org/10.1016/j.electacta.2015.09.026>.

References

- [1] B. O'Regan, M. Grätzel, A low-cost, high-efficiency solar cell based on dye-sensitized colloidal titanium dioxide films, *Nature* 353 (1991) 737–740.
- [2] M. Grätzel, Photoelectrochemical cells, *Nature* 414 (2001) 338–344.
- [3] S. Mathew, A. Yella, P. Gao, R. Humphry-Baker, F.E. Curchod/Basile, N. Ashari-Astani, I. Tavernelli, U. Rothlisberger, Md.K. Nazeeruddin, M. Grätzel, Dye-sensitized solar cells with 13% efficiency achieved through the molecular engineering of porphyrin sensitizers, *Nat Chem* 6 (2014) 242–247.
- [4] T. Perera, S. Daeneke, Z. Makuta, Y. Yu, A. Tachibana, C.A. Bäuerle, U. Ohlin, L. Spiccia, Application of the Tris(acetylacetonato) iron(III)/(II) Redox Couple in p-Type Dye-Sensitized Solar Cells, *Angew. Chem. Int. Ed.* 54 (2015) 3758–3762.
- [5] Z. Xu, D. Xiong, H. Wang, W. Zhang, X. Zeng, L. Ming, W. Chen, X. Xu, J. Cui, M. Wang, S. Powar, U. Bach, Y.-B. Cheng, Remarkable photocurrent of p-type dye-sensitized solar cell achieved by size controlled CuGaO nanoplates, *J. Mater. Chem. A* 2 (2014) 2968–2976.
- [6] S. Powar, T. Daeneke, M.T. Ma, D. Fu, N.W. Duffy, G. Götz, M. Weidelener, A. Mishra, P. Bäuerle, L. Spiccia, U. Bach, Highly Efficient p-Type Dye-Sensitized Solar Cells based on Tris(1,2-diaminoethane) Cobalt(II)/(III) Electrolytes, *Angew. Chem. Int. Ed.* 52 (2013) 602–605.
- [7] A. Yella, H.W. Lee, H.N. Tsao, C. Yi, A.K. Chandiran, M.K. Nazeeruddin, E.W.G. Diau, C.Y. Yeh, S.M. Zakeeruddin, M. Grätzel, Porphyrin-Sensitized Solar Cells with Cobalt (II/III)-Based Redox Electrolyte Exceed 12 Percent Efficiency, *Science* 334 (2011) 629–634.
- [8] T. Daeneke, T.-H. Kwon, A.B. Holmes, N.W. Duffy, U. Bach, L. Spiccia, High-efficiency dye-sensitized solar cells with ferrocene-based electrolytes, *Nat. Chem* 3 (2011) 213–217.
- [9] T. Daeneke, Y. Uemura, N.W. Duffy, A.J. Mozer, N. Koumura, U. Bach, L. Spiccia, Aqueous Dye-Sensitized Solar Cell Electrolytes Based on the Ferricyanide-Ferrocyanide Redox Couple, *Adv. Mater.* 24 (2012) 1222–1225.
- [10] M. Wang, N. Chamberland, L. Breau, J.-E. Moser, R. Humphry-Baker, B. Marsan, S.M. Zakeeruddin, M. Grätzel, An organic redox electrolyte to rival triiodide/iodide in dye-sensitized solar cells, *Nat. Chem.* 2 (2010) 385–389.
- [11] A. Hagfeldt, G. Boschloo, L. Sun, L. Kloo, H. Pettersson, Dye-Sensitized Solar Cells, *Chem. Rev.* 110 (2010) 6595–6663.
- [12] J. Gong, J. Liang, K. Sumathy, Review on dye-sensitized solar cells (DSSCs): Fundamental concepts and novel materials, *Renewable Sustainable Energy Rev.* 16 (2012) 5848–5860.
- [13] M. Grätzel, Recent Advances in Sensitized Mesoscopic Solar Cells, *Acc. Chem. Res.* 42 (2009) 1788–1798.
- [14] S. Yanagida, Y. Yu, K. Manseki, Iodine/Iodide-Free Dye-Sensitized Solar Cells, *Acc. Chem. Res.* 42 (2009) 1827–1838.
- [15] F. Odobel, Y. Pellegrin, E. Gibson, A. Hagfeldt, A.L. Smeigh, L. Hammarström, Recent advances and future directions to optimize the performances of p-type dye-sensitized solar cells, *Coord. Chem. Rev.* 256 (2012) 2414–2423.
- [16] S. Powar, Q. Wu, M. Weidelener, A. Nattestad, Z. Hu, A. Mishra, P. Bäuerle, L. Spiccia, Y.-B. Cheng, U. Bach, Improved photocurrents for p-type dye-sensitized solar cells using nano-structured nickel(ii) oxide microballs, *Energy Environ. Sci.* 5 (2012) 8896–8900.
- [17] B. Hardin, H. Snaith, M. McGehee, The renaissance of dye-sensitized solar cells, *Nat. Photon.* 6 (2012) 162–169.
- [18] M. Liang, J. Chen, Arylamine organic dyes for dye-sensitized solar cells, *Chem Soc Rev* 42 (2013) 3453–3488.
- [19] E.A. Gibson, A.L. Smeigh, L. Le Pleux, L. Hammarström, F. Odobel, G. Boschloo, A. Hagfeldt, Cobalt Polypyridyl-Based Electrolytes for p-Type Dye-Sensitized Solar Cells, *J. Phys. Chem. C* 115 (2011) 9772–9779.
- [20] L. Le Pleux, A.L. Smeigh, E. Gibson, Y. Pellegrin, E. Blart, G. Boschloo, A. Hagfeldt, L. Hammarström, F. Odobel, Synthesis, photophysical and photovoltaic investigations of acceptor-functionalized perylene monoimide dyes for nickel oxide p-type dye-sensitized solar cells, *Energy Environ. Sci.* 4 (2011) 2075–2084.

- [21] L. Li, E.A. Gibson, P. Qin, G. Boschloo, M. Gorlov, A. Hagfeldt, L. Sun, Double-Layered NiO Photocathodes for p-Type DSSCs with Record IPCE, *Adv. Mater.* 22 (2010) 1759–1762.
- [22] C.-Y. Hsu, W.-T. Chen, Y.-C. Chen, H.-Y. Wei, Y.-S. Yen, K.-C. Huang, K.-C. Ho, C.-W. Chu, J.T. Lin, Charge transporting enhancement of NiO photocathodes for p-type dye-sensitized solar cells, *Electrochim. Acta* 66 (2012) 210–215.
- [23] S. Powar, D. Xiong, T. Daeneke, M.T. Ma, A. Gupta, G. Lee, S. Makuta, Y. Tachibana, W. Chen, L. Spiccia, Y.-B. Cheng, G. Götz, P. Bäuerle, U. Bach, Improved Photovoltages for p-Type Dye-Sensitized Solar Cells Using CuCrO₂ Nanoparticles, *J. Phys. Chem. C* 118 (2014) 16375–16379.
- [24] G. Wang, W. Xing, S. Zhuo, Nitrogen-doped graphene as low-cost counter electrode for high-efficiency dye-sensitized solar cells, *Electrochim. Acta* 92 (2013) 269–275.
- [25] J. He, H. Lindström, A. Hagfeldt, S.-E. Lindquist, Dye-Sensitized Nanostructured p-Type Nickel Oxide Film as a Photocathode for a Solar Cell, *J. Phys. Chem. B* 103 (1999) 8940–8943.
- [26] T. Daeneke, Z. Yu, G.P. Lee, D. Fu, N.W. Duffy, S. Makuta, Y. Tachibana, L. Spiccia, A. Mishra, P. Bäuerle, U. Bach, Dominating Energy Losses in NiO p-Type Dye-Sensitized Solar Cells, *Adv. Energy Mater.* 5 (2015), doi:<http://dx.doi.org/10.1002/aenm.201401387>.
- [27] J. He, H. Lindström, A. Hagfeldt, S.-E. Lindquist, Dye-sensitized nanostructured tandem cell-first demonstrated cell with a dye-sensitized photocathode, *Sol. Energy Mater. Sol. Cells* 62 (2000) 265–273.
- [28] A. Nattestad, A.J. Mozer, M.K.R. Fischer, Y.B. Cheng, A. Mishra, P. Bäuerle, U. Bach, Highly efficient photocathodes for dye-sensitized tandem solar cells, *Nat. Mater* 9 (2010) 31–35.
- [29] T. Geiger, S. Kuster, J.-H. Yum, S.-J. Moon, M.K. Nazeeruddin, M. Grätzel, F. Nüesch, Molecular Design of Unsymmetrical Squaraine Dyes for High Efficiency Conversion of Low Energy Photons into Electrons Using TiO₂ Nanocrystalline Films, *Adv. Funct. Mater.* 19 (2009) 2720–2727.
- [30] G. Boschloo, L. Haggman, A. Hagfeldt, Quantification of the effect of 4-tert-butylpyridine addition to I⁻/I₃⁻ redox electrolytes in dye-sensitized nanostructured TiO₂ solar cells, *J. Phys. Chem. B* 110 (2006) 13144–13150.
- [31] Y. Xu, M.A.A. Schoonen, The absolute energy positions of conduction and valence bands of selected semiconducting minerals, *Am. Miner.* 85 (2000) 543–556.
- [32] G. Boschloo, A. Hagfeldt, Characteristics of the Iodide/Triiodide Redox Mediator in Dye-Sensitized Solar Cells, *Acc. Chem. Res.* 42 (2009) 1819–1826.
- [33] H. Tian, Z. Yu, A. Hagfeldt, L. Kloo, L. Sun, Organic redox couples and organic counter electrode for efficient organic dye-sensitized solar cells, *J. Am. Chem. Soc.* 133 (2011) 9413–9422.
- [34] H. Tian, X. Jiang, Z. Yu, L. Kloo, A. Hagfeldt, L. Sun, Efficient Organic-Dye-Sensitized Solar Cells Based on an Iodine-Free Electrolyte, *Angew. Chem. Int. Ed.* 49 (2010) 7328–7331.
- [35] H. Tian, E. Gabrielsson, Z. Yu, A. Hagfeldt, L. Kloo, L. Sun, A thiolate/disulfide ionic liquid electrolyte for organic dye-sensitized solar cells based on Pt-free counter electrodes, *Chem. Commun.* 47 (2011) 10124–10126.
- [36] J. Zhang, H. Long, S.G. Miralles, J. Bisquert, F. Fabregat-Santiago, M. Zhang, The combination of a polymer-carbon composite electrode with a high-absorptivity ruthenium dye achieves an efficient dye-sensitized solar cell based on a thiolate-disulfide redox couple, *Phys. Chem. Chem. Phys.* 14 (2012) 7131–7136.
- [37] M. L. Wang, Y. Wu, T. Ma Gao, Highly catalytic counter electrodes for organic redox couple of thiolate/disulfide in dye-sensitized solar cells, *Appl. Phys. Lett.* 98 (2011) 221102–221101–221102–221103.
- [38] J. Cong, X. Yang, L. Kloo, L. Sun, Iodine/iodide-free redox shuttles for liquid electrolyte-based dye-sensitized solar cells, *Energy Environ. Sci.* 5 (2012) 9180–9194.
- [39] T. Ono, T. Yamaguchi, H. Arakawa, Study on dye-sensitized solar cell using novel infrared dye, *Sol. Energy Mater. Sol. Cells* 93 (2009) 831–835.
- [40] N. Takeda, B.A. Parkinson, The relationship between squaraine dye surface morphology and sensitization behavior on SnS₂ electrodes, *Electrochim. Acta* 45 (2000) 4559–4564.
- [41] J.-H. Yum, P. Walter, S. Huber, D. Rentsch, T. Geiger, F. Nüesch, F. De Angelis, M. Grätzel, M.K. Nazeeruddin, Efficient Far Red Sensitization of Nanocrystalline TiO₂ Films by an Unsymmetrical Squaraine Dye, *J. Am. Chem. Soc.* 129 (2007) 10320–10321.
- [42] M. Nattestad, R. Ferguson, Y.-B. Cheng, U. Bach, Dye-sensitized nickel (II) oxide photocathodes for tandem solar cell applications, *Nanotechnology* 19 (2008) 295304–295301–295304–295309.

Thiolate/Disulfide Based Electrolytes for p-type and Tandem Dye-Sensitized Solar Cells

Satvasheel Powar,^{a,b*} Rishabh Bhargava,^c Torben Daeneke,^{d,e} Günther Götz,^f Peter Bäuerle,^f Thomas Geiger,^g Simon Kuster,^h Frank A. Nüesch,^g Leone Spiccia,^a Udo Bach^{c,d,i*}

^a School of Chemistry, Monash University, Clayton, Victoria, 3800 Australia

^b School of Engineering, Indian Institute of Technology Mandi, Mandi, Himachal Pradesh, 175001 India

^c Department of Materials Engineering, Monash University, Clayton Victoria, 3800 Australia.

^d Commonwealth Scientific and Industrial Research Organization, Materials Science and Engineering, Clayton South, Victoria 3169, Australia

^e School of Electrical and Computer Engineering, RMIT University, 3000 Melbourne, Victoria, Australia

^f Institute for Organic Chemistry II and Advanced Materials, University of Ulm, Albert-Einstein-Allee 11, 89081 Ulm, Germany.

^g Laboratory for Functional Polymers, Swiss Federal Laboratories for Materials Science and Technology (Empa), Überlandstrasse 129, 8600 Dübendorf, Switzerland

^h Institut für Lebensmittelwissenschaften, Ernährung und Gesundheit (IFNH), LFO E12.2, Schmelzbergstrasse 9, 8092 Zürich, Switzerland

ⁱ Melbourne Centre for Nanofabrication, 151 Wellington Road, Clayton, VIC 3168, Australia

ASSOCIATED CONTENT

Materials and methods

The materials (NiO, fluorine doped tin oxide coated conducting glass, SQ2 dye and the redox couple components) were purchased from commercial suppliers and used as received unless stated otherwise. PMI-6T-TPA dye was synthesized in-house.

Working electrode materials

NiO electrode preparation:

NiO nanoparticle powder was used as received from Inframat (73 wt% Ni, nominal particle size: 20 nm). All other chemicals and solvents were purchased from Sigma-Aldrich and used as received. Screen-printing pastes were prepared by mixing 8 wt % NiO, 46% ethyl cellulose solution (5 wt % in ethanol) and 46% terpineol using as-received NiO nanoparticle powder. The substrates were cleaned in an ultrasonic bath for 10 min in 5 % Hellmanex dissolved in water followed by rinsing with clean water and further sonication (10 min) in ethanol. The paste was printed on FTO glass (NSG - $8 \Omega/\square$, 4 mm thick) using a commercial semi-automatic screen printer. The thicknesses of the sintered electrodes were measured using a Veeco Dektak 6M stylus profilometer.

Just before dye-sensitization, the working electrodes were reheated to 550 °C for 10 minutes using a heat gun to remove absorbed water and organics from the NiO surface. After cooling to 60 °C the films were immersed into the dye bath. Dye deposition was achieved from a 0.2 mM

PMI-6T-TPA dye solution (see Figure 1) in DMF. After two hours of dye deposition the films were rinsed in DMF and assembled to p-DSCs.

TiO₂ electrode preparation

The TiO₂ pastes (PST-18NR) were purchased from JGC Catalysts and Chemicals. The substrates were cleaned in an ultrasonic bath for 10 min in 5 % Helmanex dissolved in water followed by rinsing with clean water and further sonication (10 min) in ethanol. The substrates were coated with a dense TiO₂ blocking layer by spray pyrolysis at 450 °C using a 7.5 wt % titanium diisopropoxide bis(acetylacetonate) in isopropanol. TiO₂ paste (PST-18R, JGC Catalysts and Chemicals) was screen printed on FTO glass (NSG - 8 Ω/□, 4 mm thick) using a commercial semi-automatic screen printer, with a 90 T mesh. One print was found to deposit 2 μm thick TiO₂ layers. The films were sintered under a stream of compressed air at 450 °C for 30 minutes followed by 15 minutes at 500 °C. After initial sintering, all films were treated with an aqueous TiCl₄ solution (20 mM, 70 °C, 30 min). The films were sintered again and stored until use. The printed transparent TiO₂ film thickness was measured to be 2 μm. The dimensions of the printed films were 4 x 4 mm (area 0.16 cm²).

Just before dye-sensitization, the working electrodes were reheated to 500 °C for 30 minutes using a heat gun to remove absorbed water and organics from the TiO₂ surface. After cooling to 60 °C the films were immersed into the dye bath. Dye deposition was achieved from a 0.2 mM SQ2 dye solution (see Figure 1b) in ethanol containing 10 mM chenodeoxycholic acid, used as a co-adsorbent. After two hours of dye deposition the films were rinsed in acetonitrile and assembled to n-DSCs.

Counter electrode preparation

For n-DSCs and p-DSCs, the counter electrode glass was cut to size and a hole was drilled (~1mm diameter) to fill in the electrolyte. The hole was drilled using a Dremmel bench drill with a dental burr. The separated counter electrodes were cleaned in ultrasonic bath following the same procedure described for the working electrodes. The prepared counter electrodes were stored in ethanol until use. The counter electrodes were coated with a drop of a 10 mM solution of hexachloroplatinic acid in isopropanol. The counter electrodes were then sintered at 400 °C for 15 minutes. For pn-DSCs, holes were drilled on TiO₂ electrodes prior to dyeing process.

PEDOT counter electrode preparation

The PEDOT counter electrodes were prepared following literature procedure.¹ The pulse potentiostatic electropolymerization of PEDOT thin films onto FTO glass substrates were carried out using a simple aqueous solution (50 mL) containing 2.0 mM 3,4-ethylenedioxythiophene monomer (ARCOS, 99%), 10 mM sodium dodecyl sulfate, and 10 mM lithium perchlorate (LiClO₄) in a three-compartment cell at ambient atmosphere, which was controlled by EC-lab software. The parameters for the electropolymerization of PEDOT were set under the pulse-on potential of 1.2 V vs. Ag/AgCl, the pulse reversal potential of 0.2 V vs. Ag/AgCl, the pulse-on period of 1 s, the pulse-reversal period of 0.5 s and total duration interval of 500 s. A Pt wire and an Ag/AgCl reference electrode were used as a counter electrode and a reference electrode, respectively. The obtained PEDOT CEs were rinsed in distilled water and dried under a cool air flow.

Device assembly

p-DSCs and n-DSCs were assembled by inserting a laser cut 25 μm thick surlyn gasket (inner dimensions 6 x 7 mm) in between the working and counter electrodes. Pneumatic finger press was used to press the working electrode while heating counter electrode. The electrolyte was vacuum backfilled in the cell cavity. The back filled hole was sealed using an aluminum-Surlyn sheet, which was prepared by heating aluminum foil with a 25 μm Surlyn sheet on a hot plate at 120 °C.

The tandem solar cells were assembled in similar way, replacing the counter electrode with pre-drilled TiO_2 working electrode. The TiO_2 electrodes and NiO electrodes were assembled with a laser cut 25 μm thick surlyn gasket (inner dimensions 6 x 7 mm) in between. Following the same procedure as p-DSCs/n-DSCs.

Rest potential measurement:

Electrochemical experiments were performed at room temperature in the glove box using a potentiostat. The redox potential of the electrolytes was determined from the potential difference between a platinum wire, immersed in the redox electrolyte, and a Ag/Ag^+ reference electrode.² The reference electrode was calibrated against the freshly prepared solution of ferrocene/ferrocenium redox couple.

Device characterization:

An Oriel sun simulator (1,000 W/m^2 Xe lamp) fitted with an AM 1.5 filter resembling the solar spectrum was used to test the photocathodes. The light intensity was calibrated with a calibrated

silicon reference diode (Fraunhofer) equipped with a KG3 filter to reduce spectral mismatch between calibrated diode and measured photocathode. Current-voltage characteristics were measured using a Keithley 2400 source meter and a custom made Lab view software.

The spectral response (IPCE) of the photocathode was measured using an Oriel 300 W Xe lamp fitted with a Cornstone monochromator and recorded on a Keithley 2400 source meter. The light intensity was quantified using a calibrated Fraunhofer reference diode.

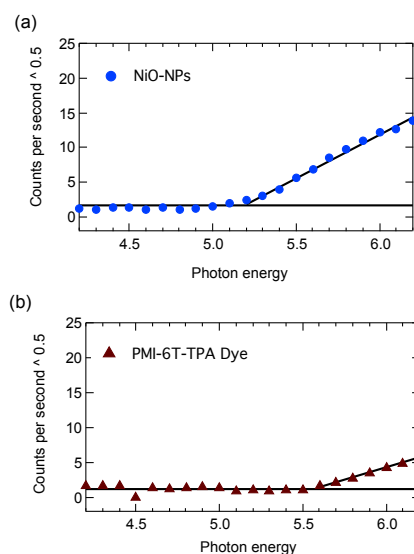


Fig S1: Photoelectron spectroscopy (PESA) measurements of ionization potential of (a) NiO and (b) sensitizer in eV (Vs Vacuum)

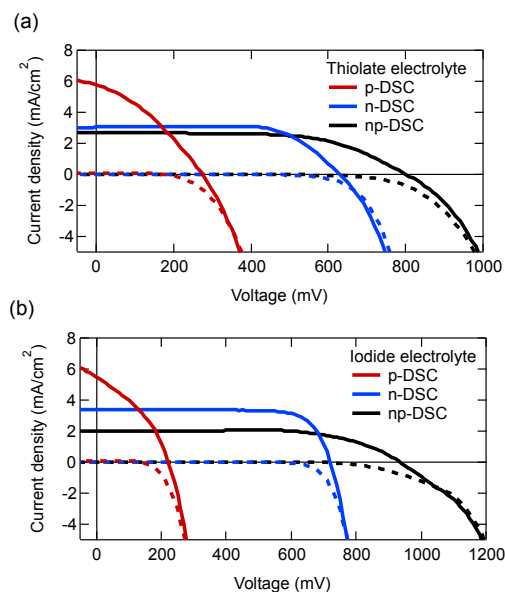


Figure S2. Photocurrent density – voltage (J-V) curves under simulated one sun (1000 W/m²) irradiation (AM 1.5 G) of p-DSC, n-DSC and tandem np-DSC using (a) a thiolate electrolyte; and (b) an iodide electrolyte. The tandem pn-DSCs and n-DSCs were illuminated through the n-

side and the p-DSCs were illuminated through p-side. Table 1 shows the corresponding the J-V characteristics.

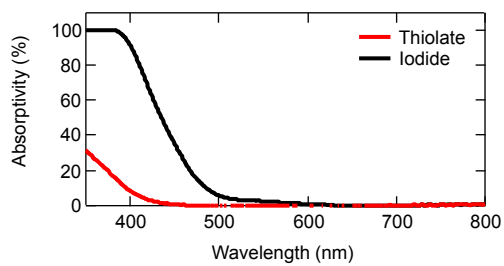


Figure S3. Absorptivity spectra of thiolate (red line) and iodide (black line) electrolytes with path length of 22.5 μm , corresponding to a typical electrolyte layer thickness in DSCs.

The photocurrent (J_{SC}) calculations:

The theoretical photocurrent densities (J_{SC}) generated by dye-sensitized solar cells can be calculated using equation (1), where LHE is light harvesting efficiency. For LHE calculations equation (2), detailed optical analysis was carried on TiO_2 and NiO films before and after dyeing process ($A_{(SC)}(\lambda)$) and $A_{(Dyed SC)}(\lambda)$ respectively. The dye absorption on the film ($A_{(dye)}(\lambda)$) was calculated by subtracting absorption of the semiconductor [$A_{(SC)}(\lambda)$] from $A_{(dyed SC)}(\lambda)$. The electrolyte absorptions were measured with a $22.5 \mu m$ path length.

Based on the optical analysis, film absorptions were normalized to $1 \mu m$ thick films. The expected light-harvesting efficiencies as a function of film thickness for both types of sensitized semiconductor electrodes were calculated. Assuming APCE = 1, theoretical maximum photocurrents ($J_{SC \text{ max}}$) were calculated using equation (3) as a function of film thickness. The p-DSC and n-DSC IPCEs of known film thickness were measured and compared with equation 3 to calculate APCE values for both n-DSC and p-DSC. The calculated APCE_{MAX} values for n-DSC and p-DSC are shown in table S3.

$$J_{SC} = \frac{e}{hc} \int \phi_p \text{AM1.5G}(\lambda) \cdot \text{LHE}(\lambda) \cdot \phi_{inj} \cdot \phi_{cc} \cdot d\lambda \quad (1)$$

where e is electric charge, h is Planck's constant, c is speed of light, ϕ_p is photon flux, LHE is light harvesting efficiency, ϕ_{inj} is charge injection efficiency and ϕ_{cc} is charge collection efficiency.

$$\text{LHE}_{(dye)}(\lambda, d) = \frac{A_{(Dye)}(\lambda)}{A_{(Dyed SC)}(\lambda)} \cdot (1 - 10^{-\tilde{A}_{(Dyed SC)}(\lambda) \cdot d}) \quad (2)$$

$$\text{When APCE} = \phi_{inj} \cdot \phi_{cc} = 1$$

$$J_{SC}^{max}(d) = \frac{e}{hc} \int \phi_p \text{AM1.5G}(\lambda) \cdot LHE(\lambda, d) \cdot d\lambda \quad (3)$$

$$\text{Since } LHE(\lambda) \cdot \phi_{inj} \cdot \phi_{cc} = IPCE(\lambda) \quad (4)$$

$$J_{SC}^{IPCE} = \frac{e}{hc} \int \phi_p \text{AM1.5G}(\lambda) \cdot IPCE(\lambda) \cdot d\lambda \quad (5)$$

$$APCE(\lambda) = \phi_{inj} \cdot \phi_{cc} = \frac{IPCE(\lambda)}{LHE(\lambda)} \quad (6)$$

$$J_{SC}^{APCE}(d) = \frac{e}{hc} \int \phi_p \text{AM1.5G}(\lambda) \cdot LHE(\lambda, d) \cdot APCE(\lambda) \cdot d\lambda \quad (7)$$

Where $A_{(\text{dyed SC})}(\lambda)$ are absorption of the dyed semiconductor. $\tilde{A}_{(\text{Dyed SC})}(\lambda)$ is absorption of dyed NiO film per μm and d is the film thickness in μm .

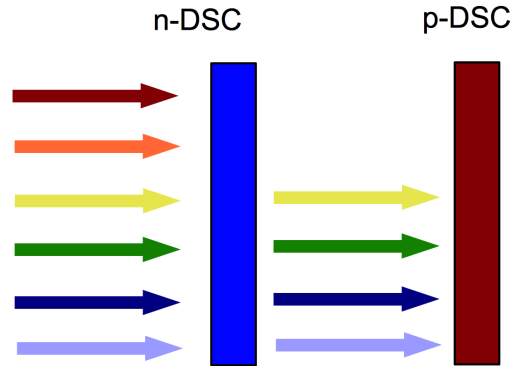


Fig S4. Schematic representation of pn-DSC absorption with n-DSC and p-DSC electrodes

Figure S4 shows a tandem structure for pn-DSC with illumination through photoanode (TiO_2) side. In tandem structures, the light reaching the second electrode was estimated by subtracting absorptivity of first electrode and absorptivity of electrolyte from incident light as a function of wavelength. The light harvesting efficiencies of second electrodes were recalculated according to the corrected incident light. Theoretical J_{SC} s were estimated from the calculated LHE and APCE values as a function of film thickness. According to the Kirchoff's circuit law, the photocurrent

of a tandem solar cell is governed by, low photocurrent producing electrode. The minimum estimated photocurrents was recorded for a given TiO_2 and NiO film thicknesses. Based on the different film thickness matrix, the photocurrents were estimated and a countour was plotted.

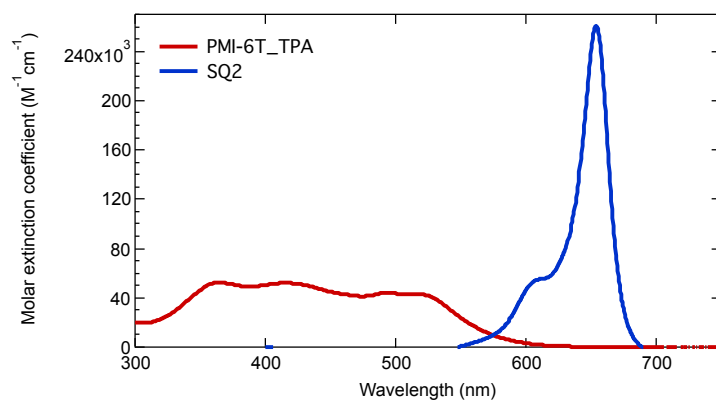


Figure S5. Absorption spectra of p-DSC dye (PMI-6T-TPA in dichloromethane) and n-DSC dye (SQ2 in EtOH) used in this study

Table S1. The experimentally determined APCE values for p-DSCs sensitized with PMI-6T-TPA and n-DSCs sensitized with SQ2 employing thiolate and iodide electrolytes.

	Iodide electrolyte	Thiolate electrolyte
p-DSC	0.95	0.92
n-DSC	0.40	0.38

Table S2. Photovoltaic performance parameters for pn-DSCs under 100% sun simulated sunlight (1000 W/m², AM1.5 G) using 1.6 μm TiO₂ and 2 μm NiO. The tandem pn-DSCs and n-DSCs were illuminated through the n-side (TiO₂). The effect of Li⁺ ions on the device performance of pn- DSCs was studied by comparing the iodide-based electrolyte with its analogue containing Li⁺ ions.

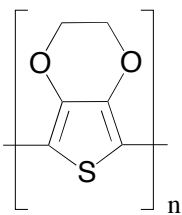
	Iodide electrolyte	Lithium added iodide electrolyte
	pn-DSC	pn-DSC
V _{OC} (mV)	936 ± 16	750 ± 29
J _{SC} (mA/cm ²)	2.6 ± 0.1	2.6 ± 0.2
Fill Factor	0.52 ± 0.04	0.60 ± 0.01
Efficiency (%)	1.28 ± 0.01	1.18 ± 0.01

Composition of iodide electrolyte: 0.03 M iodine, 0.6 M 1-butyl-3-methylimidazolium iodide, 0.5 M 4-tert-butylpyridine and 0.1 M guanidinium thiocyanate in 85:15 acetonitrile: valeronitrile.

Composition of Li added iodide electrolyte: 0.03 M iodine, 0.6 M 1-butyl-3-methylimidazolium iodide, 0.5 M 4-tert-butylpyridine, 0.1 M guanidinium thiocyanate and 0.05 M lithium in 85:15 acetonitrile: valeronitrile

Table S3. Photovoltaic performance parameters for p-DSCs, n-DSCs and pn-DSCs under 10% sun simulated sunlight (100 W/m², AM1.5 G) using 2 μm TiO₂ and 1.8 μm NiO. The tandem pn-DSCs and n-DSCs were illuminated through the n-side (TiO₂) and the p-DSCs were illuminated through the p-side (NiO).

	Thiolate electrolyte			Iodide electrolyte		
	p-DSC	n-DSC	pn-DSC	p-DSC	n-DSC	pn-DSC
V _{oc} (mV)	224 ± 9	507 ± 7	663 ± 20	175 ± 3	657 ± 10	819 ± 19
J _{sc} (mA/cm ²)	0.79 ± 0.08	0.31 ± 0.05	0.30 ± 0.04	0.75 ± 0.04	0.35 ± 0.01	0.27 ± 0.07
Fill Factor	0.40 ± 0.04	0.62 ± 0.04	0.69 ± 0.03	0.41 ± 0.01	0.78 ± 0.01	0.70 ± 0.01
Efficiency (%)	0.71 ± 0.07	0.98 ± 0.26	1.35 ± 0.08	0.52 ± 0.03	1.78 ± 0.05	1.55 ± 0.06



Poly(3,4-ethylenedioxythiophene)

Figure S6. Chemical structure of PEDOT [poly(3,4-ethylenedioxythiophene)]

References:

1. Xiao, Y.; Lin, J.-Y.; Tai, S.-Y.; Chou, S.-W.; Yue, G.; Wu, J. *J. Mater. Chem.* **2012**, 22, (37), 19919-19925.
2. Boschloo, G.; Hagman, L.; Hagfeldt, A. *J. Phys. Chem. B* **2006**, 110, (26), 13144-13150.